Beam-shape Coefficients, Localization Principle and Excitation of Resonances in Mie's Scattering

波束形狀係數、局域化原理及米氏散射中的共振激發

FU, Pengpeng

傅芃芃

A Thesis Submitted in Partial Fulfillment
of the Requirements for the Degree of
Doctor of Philosophy
in
Physics

The Chinese University of Hong Kong

June 2010

ProQuest LLC
789 East Eisenhower Parkway
P.O. Box 1346
Ann Arbor, MI 48106-1346

Thesis/Assessment Committee

Professor YOUNG, Kenneth (Chair)
Professor LAI, Hon Ming (Thesis Supervisor)
Professor LEE, Wing Kee (Committee Member)
Professor PU, Xiaoyun (External Examiner)

Abstract

Exact and distance-independent expressions for beam-shape coefficients (BSC's) in various cases are obtained. For a weakly focused beam in the two-dimensional (three-dimensional) case, the expression is shown equal (linearly related) to the value of the beam field at the distance of m/k ($\sqrt{l(l+1)}/k$) from the origin, where $m(l)$ is the azimuthal (principal) angular momentum number and k is the wavenumber. This provides a rigorous foundation for and a better understanding of the localization principle of van de Hulst. Furthermore, it gives corrections to the principle if the beam is more focused. With the knowledge of the asymptotic behavior of the positions and widths (or quality value) for the morphology-dependent resonances (MDR's) in Mie's scattering, the results are applied to discuss and answer questions regarding the excitation of high-Q MDR's by good collimated wave beams focused at positions essentially off the surface of the sphere.

摘　要

針對不同情況，本文得到了與距離散射中心位置無關的波束形狀因子。對于一束二維（三維）的弱聚焦波束，我們的近似表達式正比于該波束在距離坐標原點 m/k ($\sqrt{l(l+1)}/k$)處的波場。其中 m (l)分別爲方位（主）角動量量子數，k 爲波束的波數。這一方面爲 van de Hulst 所提出的局域性原理提供了更嚴格的理論依據，同時也便于我們對該原理有更深入的理解。另外，有關結果也預示了該局域性原理的高階誤差。在對 MDR 共振位置、寬度有深入瞭解的基礎上，我們也嘗試回答了波束入射在散射對象表面外面的時候如何引起共振激發的問題。

Contents

List of Figures

Chapter 1

Introduction

The Mie scattering, which refers to the scattering of plane electromagnetic waves by an isotropic and homogeneous sphere, is a topic of long history [1–5]; it is sometimes called the Lorenz-Mie scattering because Lorenz studied a similar problem earlier in the context of scattering of sound waves [6]. This problem has attracted much interest in recent decades [5, 7–11], mainly because of the appearance of resonances, which can be readily demonstrated with the advent of lasers and sophisticated diagnostics, and leads to studies and applications in various areas, including lasing [12, 13], particle sizing [14, 15], Raman scattering [16, 17], optical levitation [18], etc.

Such resonances in fact come from the exceptionally large values of the coefficients at certain size parameters $s \equiv ka = 2\pi a/\lambda$ (a being the radius of the sphere, and λ the wavelength). These coefficients, each labeled by two angular momentum numbers (principal l and azimuthal m) are those of the partial-wave terms in the series solutions originally obtained by Mie for the scattered field and the internal field. Physically, the resonances are due to the tunneling of the incident wave into the sphere, as circumnavigating waves near the sur-

face, which undergo almost total internal reflection and get enhanced through phase matching. They are called morphology-dependent resonances (MDR's), whispering gallery modes (WGM's), or quasi-normal modes (QNM's), by different groups of people in the area.

Mie's theory has been generalized to the scattering of wave beams, also called the generalized Lorenz-Mie theory (GLMT) [6]. This generalization is needed not only because of laser beams being used in practice, but more importantly, because of the discovery by experiments [19, 20] and numerical simulations [21, 22] that the effectiveness of resonance excitation depends on where the beam is focused relative to the sphere. Such effective excitation has been explained by the localization principle (LP) of van de Hulst [3] in the extended version [23] which states that a partial-wave term of angular momentum number (or order) l corresponds to a ray passing the origin at a distance $(l+\frac{1}{2})\lambda/2\pi$ [3] and the ray can be off the surface. Under this principle, geometric optics (a ray) and wave optics (a partial-wave term of an order) are connected. Yet the principle is heuristic and there is obviously a need for a rigorous basis.

For an incident wave beam, there are coefficients of the partial-wave terms in the expansion for the beam field which, unlike the case of an incident plane wave, are generally different for different angular momentum numbers; they have been called the beam shape coefficients (BSC's). Relation between the BSC and the LP has been pointed out before, but only in the context of applying the latter to obtain an approximation of the former.

It is the purpose of this thesis to study the BSC and its relation to the LP in a rigorous manner and, furthermore, how it can be applied to explain the excitation of resonances by off-center or even off-surface wave beams.

For simplicity, we first study such problems in the two-dimensional (2–D) context in Chapter 2. Along the way we also obtain asymptotic formulas for the positions and widths of the high-quality (high-Q) resonances.

In chapter 3, the study is extended to the 3-dimensional (3–D) case, where both scalar wave beams and laser beams are considered. Of course, the vector nature of the latter beam fields is stressed.

The two chapters, albeit related, are written relatively self-contained. Each has an introduction of its own.

Throughout the paper, we have adopted the terminology and notations commonly used in quantum mechanics, which are also similar to those used by Jackson [24] and Young et al. [25]

Chapter 2

Beam-shape Coefficients, Localization Principle and Excitation of Resonances in Mie's Scattering — a Two-dimensional Study

Here we study how the beam-shape coefficient is related to the localization principle of van de Hulst and its relevance to the excitation of morphology-dependent resonances (MDR's) by off-surface laser beams in the two-dimensional context.

First, we obtain asymptotic formulas for the position and width of MDR's. We find that, for high-Q MDR's, the angular momentum number m is between s and ns as expected, where n is the refractive index of the sphere. In addition, we show that the Q value basically increases exponentially with the size

parameter, and this will be useful for our discussion on the excitation. Here we follow closely the method of Lam et al. [26] for the 3-D Mie scattering. The formula for the position, given by Eq. (2.9), is almost identical to that of Lam et al. This is not a surprise in view of the same physics involved. On the other hand, the formulas for the width, given by Eq. (2.13) for the two states of wave polarization and which to our knowledge have not appeared in the literature before, have the two-dimensional characteristics. These formulas should be useful in the interpretation and understanding of the resonance phenomena in cylindrical micro-cavities and the coupling between optical fibers and/or micro-disks in photonic circuitry.

Second, we consider an incident beam in either state of wave polarization and derive an exact and distance-independent expression for the BSC which, to first-order approximation in small angle of beam divergence, reduces to a simple formula, given by Eq. (2.24). This formula clearly states that the BSC of angular momentum number m is equal to the incident beam field at the perpendicular distance of m/k. This, with proper modification, essentially gives the content of the localization principle of van de Hulst, in its original or extended version. The simplicity of the beam-shape coefficient will certainly save a lot of labor in numerical computations and modelings in problems of scattering by a light beam. Moreover, we have shown the limitation of the principle and made correction to it in the case of a more focused beam.

Because m lies between s and ns and because of our approximate BSC formula, high-Q resonances are most efficiently excited by beams focused at distances between a and na, which are off the surface. There is the interesting question here, namely, how to interpret the excitation of a high-Q MDR in the sphere by an essentially off-surface laser beam, especially in the limit of short

wavelength? This is discussed and answered in the last section.

2.1 Positions and widths/Q-values of MDR's

We first set up the formulas and notations for later convenience. Taking the cylinder axis as the z-axis and the incident wave along the y-direction, it is well known that the incident, internal and scattered electric (magnetic) fields, all having only the z-component for the TE-polarization (TM-polarization) case, are respectively given by

$$F_{inc} = \exp(iky) = \sum_m J_m(kr)\exp(im\phi) \ , \tag{2.1}$$

$$F_{int} = \sum_m a_m J_m(nkr)\exp(im\phi) \ , \tag{2.2}$$

and

$$F_{sca} = \sum_m c_m H_m(kr)\exp(im\phi) \ , \tag{2.3}$$

where the common time-factor $\exp(-i\omega t)$ has been omitted for simplicity, r and ϕ are the polar coordinates in the xy-plane, the sum is over all positive and negative integers of m including 0, J_m is the Bessel function, H_m (superscript omitted for simplicity) is Hankel function of the first kind with out-going wave at infinity, m is the mode number or the angular momentum index, and the coefficients are

$$a_m = \frac{2i}{\pi s D_m(s)} \ , \tag{2.4}$$

and

$$c_m = -\frac{J_m(ns)J'_m(s) - nPJ_m(s)J'_m(ns)}{D_m(s)} \ , \tag{2.5}$$

with the denominator function defined by

$$D_m(s) = J_m(ns)H'_m(s) - nPH_m(s)J'_m(ns) \ . \tag{2.6}$$

Note that

$$P = 1 \qquad \text{or} \qquad 1/n^2 \tag{2.7}$$

for the TE-polarization case or the TM-polarization case, respectively, and the prime sign in J'_m and H'_m means a derivative of the function with respect to the argument and that each $J_m \exp(im\phi)$ or $H_m \exp(im\phi)$, together with the time-factor, is called a partial wave of mode number m in the solution.

2.1.1 Positions

Now the positions of the MDR's are determined by the zeros of the imaginary part of the denominator or

$$nPJ'_m(ns)/J_m(ns) = Y'_m(s)/Y_m(s) \ , \tag{2.8}$$

which has the same form as (2.1b) in [26]. The asymptotic position $s_{m,i}$ of mode number m and radial order number i is therefore given by

$$\begin{aligned} ns_{m,i} = m + \alpha_i \left(\frac{m}{2}\right)^{1/3} - \frac{P}{\sqrt{1-1/n^2}} + \frac{3{\alpha_i}^2}{20}\left(\frac{2}{m}\right)^{1/3} \\ - \frac{P(1-2P^2/3)\alpha_i}{2\sqrt{(1-1/n^2)^3}}\left(\frac{2}{m}\right)^{2/3} + \mathrm{O}(1/m) \end{aligned} \tag{2.9}$$

for large m, where α_i's are the roots of the Airy function $\mathrm{Ai}(-z)$ already tabulated in [26]. It is exactly the same as that by Lam et al. if m is replaced by

$l+1/2$, where l is the mode number or the principal angular momentum number in the 3-D case. The similarity is not a surprise in view of the same physical situation where the wave enhances itself through internal reflections along a big circle and phase matching. Note that the electric (magnetic) field for the TE-polarization (TM-polarization) case in the 3-D Mie scattering is parallel to the direction of the "angular momentum" and therefore perpendicular to the plane of the big circle, same as in our 2D case.

2.1.2 Widths and Q-values

The width of a resonance is related to the leakage. It may be determined by essentially switching off the incident wave, hence leaving only the internal wave and the scattered wave. The boundary conditions then require a vanishing denominator function in Eq. (2.6), which admits complex solutions for the size parameter. The imaginary part of the solution simply gives the half width, whereas the real part, for tiny leakage, should be very close to the position in Eq. (2.9), to be indicated by s_0 in the following. We follow the method of Lam et al. and introduce the mismatch function of complex z

$$M(z) \equiv H'_m(z)/H_m(z) - PnJ'_m(nz)/J_m(nz) \ . \tag{2.10}$$

The root of it, z_0, which obviously satisfies $D_m(z) = 0$, gives the complex solutions. For tiny leakage, $s_0 - z_0$ is small so that we have $M(s_0) = M'(z_0)\ (s_0 - z_0)$ to first order in the smallness. Now, use of the Wronskian of Bessel's functions leads exactly to

$$M(s_0) = -\frac{2}{\pi s_0 Y_m(s_0) H_m(s_0)} \ , \tag{2.11}$$

while use of the Bessel differential equation gives, for the TE-polarization case,

$$M'(z_0) = n^2 - 1 \tag{2.12a}$$

exactly and, for the TM-polarization case,

$$M'(z_0) = (n^2 - 1)\left[(m/ns_0)^2 + (Y'_m(s_0)/Y_m(s_0))^2\right] . \tag{2.12b}$$

The imaginary part of z_0, which is negative as expected, can therefore be obtained to yield the following full-width at half maximum (FWHM) for the MDR of mode number m and order number i

$$\Gamma_{m,i} = \frac{4}{\pi(n^2-1)Ns|H_m(s)|^2} , \tag{2.13}$$

with

$$N = 1 \quad \text{or} \quad \left(1 + 1/n^2\right)\cosh^2\xi - 1 \tag{2.14}$$

for the TE-polarization case or the TM-polarization case, respectively, where we have introduced a convenient parameter ξ through the hyperbolic cosine by

$$\cosh\xi = m/s , \tag{2.15}$$

and have approximated $Y'_m(s)/Y_m(s) = -\sinh\xi$ [See (2.6b) in [26] or [27] assuming a finite $\coth\xi$], and s in all the equations refers to the corresponding position of the resonance in Eq. (2.9). These widths have the 2D characteristics and are slightly different from the 3-D counterparts. For example, we have $2/\pi s$ instead of $1/s^2$ because of the difference in the Wronskians, and we have the (cylindrical) Bessel function instead of the spherical Bessel function.

The difference is not a surprise in view of the physical situation where the circumnavigating wave "sees" on its sides different curvatures of the interface in the two different cases. We have also numerically computed the widths and hence the Q values (defined by s/Γ) of the MDR's for a number of cases. To show the results and for comparison with our asymptotic formula, we give in Fig. 2.1 the semi-log values of $Q_{m,i}/s_{m,i}$ (i.e., $1/\Gamma_{m,i}$) versus s for a number of m's and i's for the TE-polarization case, with the index of refraction $n = 1.33$. The points, represented by different little symbols (stars, diamonds, squares, triangles and circles) each for a mode number m, are the numerically computed results. Only MDR's with $Q/s > 10$ in the range are shown. The solid lines are plotted according to our asymptotic formula Eq. (2.13), each for a fixed m and with s increasing from $s \sim m/n$; they obviously start from their respective highest values at $i = 1$ and decrease rapidly with s. The dotted lines are plotted for each i according to the following further simplified result [27]

$$1/\Gamma_{m,i} = \frac{n^2 - 1}{2} N \frac{\exp[2m(\xi - \tanh\xi)]}{\sinh\xi}. \tag{2.16}$$

which itself already shows the exponential dependence on m or s asymptotically in view of the relatively slow variation of ξ. The approximate "straightness" of the dotted lines is therefore not a surprise. Obviously, the line for $i = 1$ gives the largest Q/s. For $m = 100$, the Q/s-value is as large as 2×10^7, and exponentially larger for larger m! The comparison is very satisfactory. We note that Q/s is larger for smaller s in the range between m/n and m and this is really due to the effect of the Hankel function in the formula. The graph for the TM case have similar features.

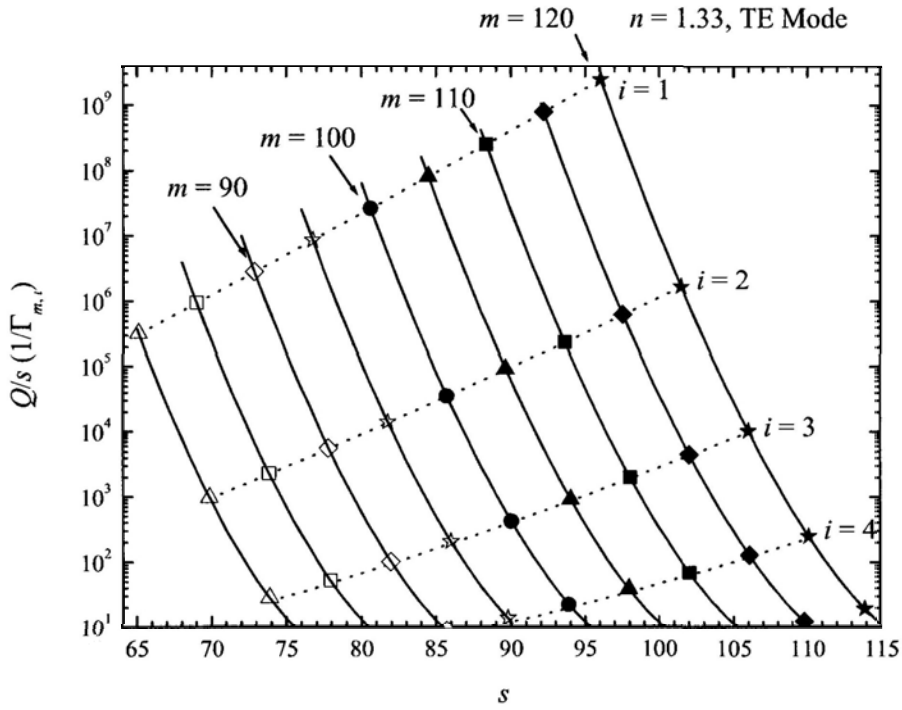

Figure 2.1: Semi-log graph of Q/s vs s for a number of m's and i's for the TE case. The points (given by the stars, diamonds, squares, triangles and circles) are the numerically computed values. Solid lines are from Eq. (2.13) and the dashed lines from Eq. (2.16).

2.2 Beam-shape coefficient and the localization principle of van de Hulst

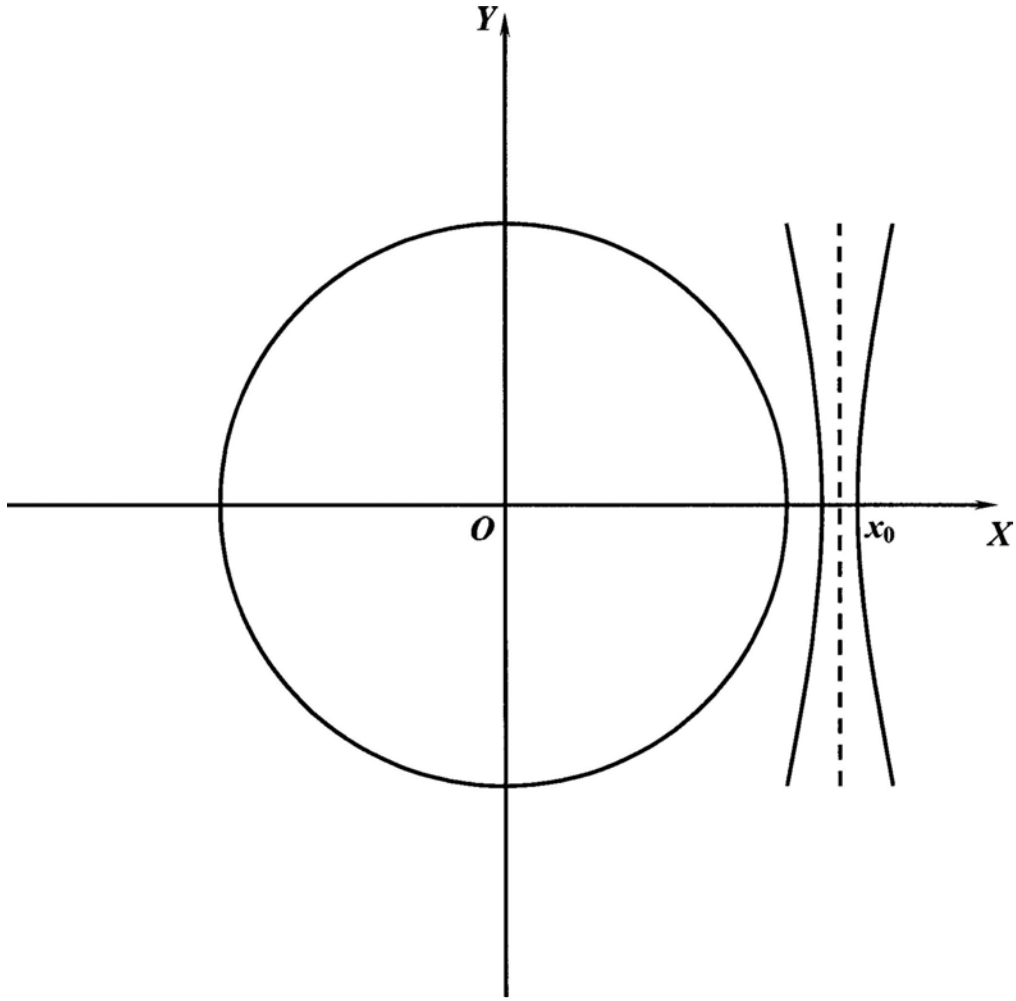

Figure 2.2: Sketch of the cross-section of a cylinder with its axis taken as the z-axis, and an incident beam focused att $(x_0, 0)$.

We now consider a 2D incident laser beam in either state of polarization, propagating mainly along the y-direction and focused at a point $\mathbf{r}_0 \equiv (x_0, y_0)$. The cross-section of the cylinder with the beam for a particular case of $y_0 = 0$

is shown schematically in Fig. 3. The field (electric for the TE-polarization case or magnetic for the TM-polarization), having only the z-component, is independent of z and can always be expressed as a linear superposition of plane wave solutions as follows

$$F_{inc}(x,y) = \int_{-k}^{k} \tilde{F}(k_x;\mathbf{r}_0)\exp(ik_x x + ik_y y)dk_x \ , \tag{2.17}$$

where $\tilde{F}(k_x;\mathbf{r}_0)$, which contains $\mathbf{r}_0$ as a parameter, is any function of k_x, $k_y = \sqrt{k^2 - k_x^2}$, and the time-factor has again been omitted. Note that, with the integration limits at $\pm k$ (i.e., $\pm\omega/c$), we have excluded component waves decaying along the y-direction; such excluded waves are believed not present in any wave beam propagating in free space.

The exponential function in the integral can now be expressed in terms of the partial waves like that in Eq. (2.1) except that the angle ϕ is now replaced by $\phi + \gamma$, where γ is the angle of the wave-vector relative to the y-axis, i.e.,

$$\sin\gamma = k_x/k \ . \tag{2.18}$$

Subsequently, we have

$$F_{inc}(x,y) = \sum_m \beta_m J_m(kr)\exp\left(im\phi\right) \ , \tag{2.19}$$

which is the same as that in Eq. (2.1) except for the additional factor, called the beam-shape coefficient (BSC), given by

$$\beta_m = \int_{-k}^{k} \tilde{F}(k_x;\mathbf{r}_0)\exp(im\gamma)dk_x \ . \tag{2.20}$$

For a perfect circular surface, the partial waves are independent of one another and, furthermore, each partial wave in the incident field is accompanied by the corresponding partial waves in the internal and scattered fields through the boundary conditions. Therefore, the internal and the scattered fields are the same as those in Eq. (2.2) and Eq. (2.3) except for the same additional factor, i.e.,

$$F_{int}(x,y) = \sum_m \beta_m a_m J_m(nkr) \exp(im\phi) \tag{2.21}$$

and

$$F_{sca}(x,y) = \sum_m \beta_m c_m H_m(kr) \exp(im\phi) \ . \tag{2.22}$$

These expressions simply show that the excitation of any MDR of a mode number m, besides the crucial dependence on the right size parameter s at which the coefficients a_m and c_m are significantly large, depends also on the value of the corresponding BSC.

2.2.1 Approximate formula for BSC

From Eq. (2.18), the following series expansion

$$\gamma = \frac{k_x}{k} + \frac{1}{6}\left(\frac{k_x}{k}\right)^3 + \frac{3}{40}\left(\frac{k_x}{k}\right)^5 \ldots \ . \tag{2.23}$$

is well-known. If only the first term is kept, the integral in Eq. (2.20) is exactly the same as that in Eq. (2.17) at $x = m/k$ and $y = 0$, yielding a remarkably simple approximate formula as follows

$$\beta_m = F_{mc}(m/k, 0) \ . \tag{2.24}$$

So the BSC of angular momentum number m in the TE (TM) case is simply equal to the value of the beam electric (magnetic) field at the perpendicular distance m/k! One obvious implication regarding the excitation of a high-Q MDR of number m is that, in addition to the crucial requirement of the right size parameter, one has to require the beam to be focused at the right distance, namely, a perpendicular distance m/k, from the cylinder axis or, in the language of quantum mechanics, to require the beam to have the right "angular momentum". Furthermore, because a high-Q MDR has its m number lying in between s and ns, its excitation is most effective if the beam is focused at a point between a and na which is essentially outside the surface of the cylinder. This is precisely the prevailing argument regarding excitation by beams using the (extended) localization principle of van de Hulst. Here we have provided a general yet rigorous derivation of it.

What is the condition for the validity of the above formula? Of course we have to require a small angle of beam divergence, i.e., $kw \gg 1$, where w is the size of the beam waist. Moreover, because it is $m\gamma$ appearing as a phase factor in Eq. (2.20), we have to require

$$m \ll (kw)^3 \tag{2.25}$$

in addition.

What is the correction to the approximate formula? This can be answered qualitatively by rewriting the first two terms in Eq. (2.23) as

$$\gamma \simeq \frac{k_x}{k}\left(1 + \frac{1}{6(kw)^2}\right) \tag{2.26}$$

where we have approximated $(k_x/k)^2$ by $1/(kw)^2$. This leads to

$$\beta_m \simeq F_{inc}\left(\frac{m}{k} + \frac{m}{6k^3w^2}, 0\right) , \tag{2.27}$$

meaning a largest BSC of m number for a beam focused at a position slightly *farther* than m/k. This correction is not negligible if m is as large as k^3w^3.

The localization principle of van de Hulst states the correspondence of a partial wave of m to a ray passing the origin at a distance m/k. This idea comes from the analogy of an electron passing by the center with angular momentum $l\hbar$ and linear momentum $\hbar k$ in quantum mechanics so that l/k is the distance of the electron if thought localized. There is a question in the statement, namely, a term of order m is a widespread wave, and so how it can correspond to a localized ray. It turns out that our approximate BSC can answer this question and thus provide a better understanding of the principle.

A ray is really a good beam of waist size (w, say) much greater than the wavelength, i.e., $kw >>> 1$. If the beam is focused at $x_0 \gg w$ from the origin, it has a spread of angular momentum from $k(x_0 - w)$ to $k(x_0 + w)$, i.e., m in the summation for the beam field, given by Eq. (2.19), need only cover this range, the BSC's for m outside the range being negligibly small. So, it is not that one partial wave of m corresponds to the ray but really that many partial waves of neighboring m's around the average $\bar{m} = kx_0$ correspond to the ray passing the origin at a distance $\bar{m}/k$. With this understanding, we may say that the localization principle of van de Hulst comes out naturally from the BSC to first-order approximation in small angle of divergence.

2.2.2 An example for exact BSC

If we take

$$\tilde{F}(k_x; \mathbf{r}_0) = \exp(-ik_x x_0) \quad \text{for} \quad k_x < k_d < k \tag{2.28}$$

and zero otherwise, meaning a beam focused at $(x_0, 0)$ and of a square Fourier-transform profile, the field in Eq. (2.17) along the x-axis can be easily evaluated to be

$$F_{inc}(x, 0) = 2\sin[k_d(x - x_0)]/(x - x_0) \tag{2.29}$$

which is recognized as the field in the (2-D) single-slit diffraction. The integral in Eq. (2.20) can then be exactly evaluated to yield

$$\beta_m = k \sum_{m'} J_{m'}(kx_0) \left[\frac{\sin(m - m' + 1)\gamma_d}{m - m' + 1} + \frac{\sin(m - m' - 1)\gamma_d}{m - m' - 1} \right] \tag{2.30}$$

where $\gamma_d \equiv \sin^{-1}(k_d/k)$ is the (half) angle of beam divergence (or convergence).

It is now of interest to plot β_m versus kx_0 and examine the variation around $kx_0 = m$ for a number of γ_d's. Moreover, we can compare it with

$$\beta_m = 2k \frac{\sin[(m - kx_0)\sin\gamma_d]}{m - kx_0} \tag{2.31}$$

obtained from the approximate formula. The results are shown in Fig. 2.3 for $m = 50, 70, 100$ with $\gamma_d = 15°$, and in Fig. 2.4 for $m = 50, 70, 90$ with $\gamma_d = 30°$, respectively. The solid lines give the exact results according to Eq. (2.30) and the dashed lines give the approximate results according to Eq. (2.31). We see the best agreement of the two curves for the smaller $\gamma_d = 15°$ and the smaller $m = 50$, as expected. In addition, the exact focus position for maximum BSC is always larger than the corresponding one given by the approximate formula.

This is also expected from Eq. (2.27).

Obviously, the approximate BSC always has its maximum if the beam focus x_0 is equal to m/k. It is therefor of interest to plot the exact focus position for maximum BSC versus m. The results are given by the points in Fig. 2.5 for $\gamma_d = 15°$, and in Fig. 2.6 for $\gamma_d = 30°$, where the straight line gives kx_0 for maximum BSC according to the approximate formula. We see that the points lie almost completely on the straight line for $\gamma_d = 15°$, while the points are slightly above the straight line for $\gamma_d = 30°$ and for larger m numbers. Again, these results are expected.

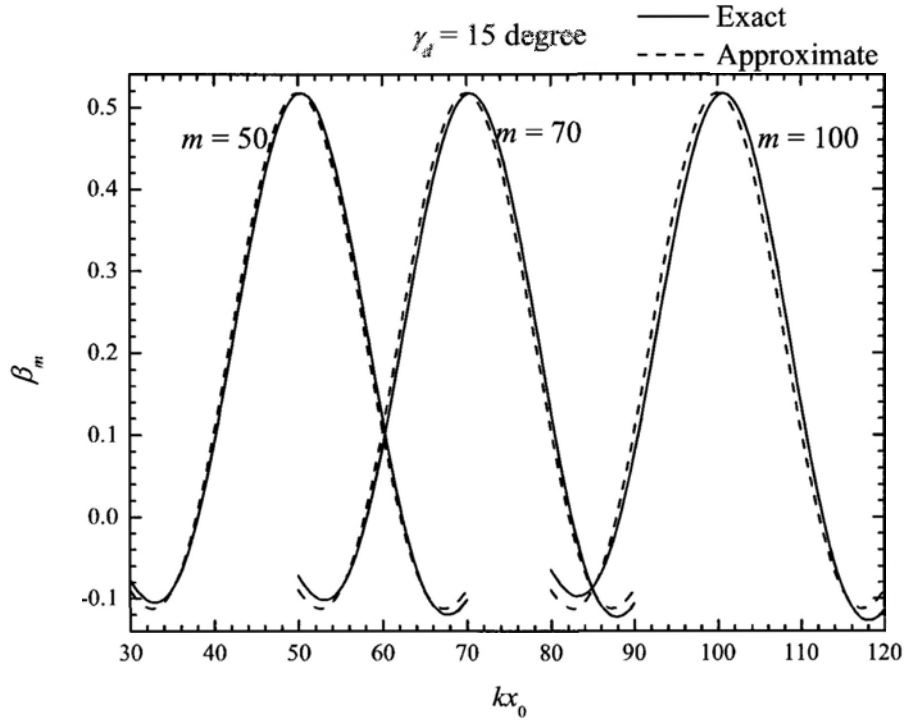

Figure 2.3: Variation of β_m versus kx_0 for $m = 50$, 70, 100 with $\gamma_d = 15°$.

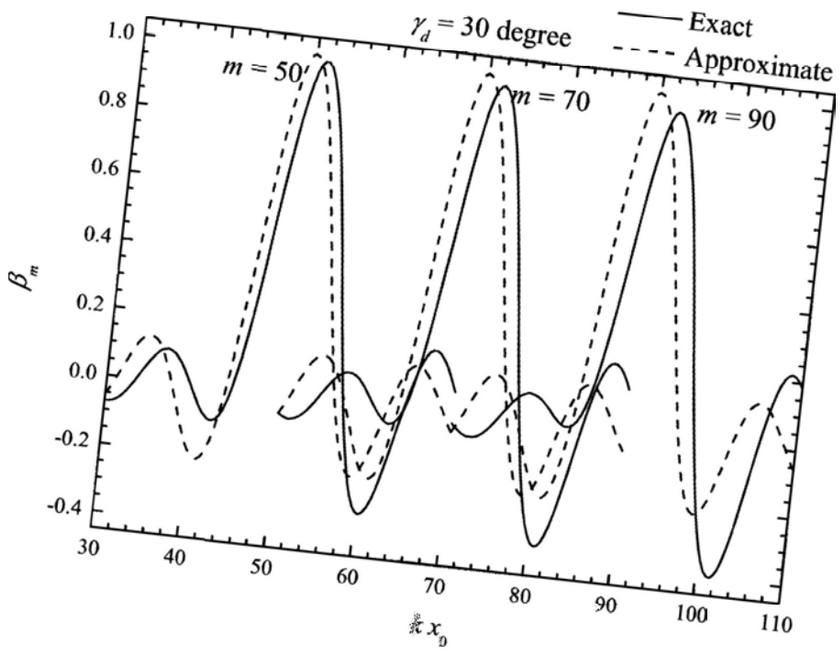

Figure 2.4: Variation of β_m versus kx_0 for $m = 50$, 70, 90 with $\gamma_d = 30°$.

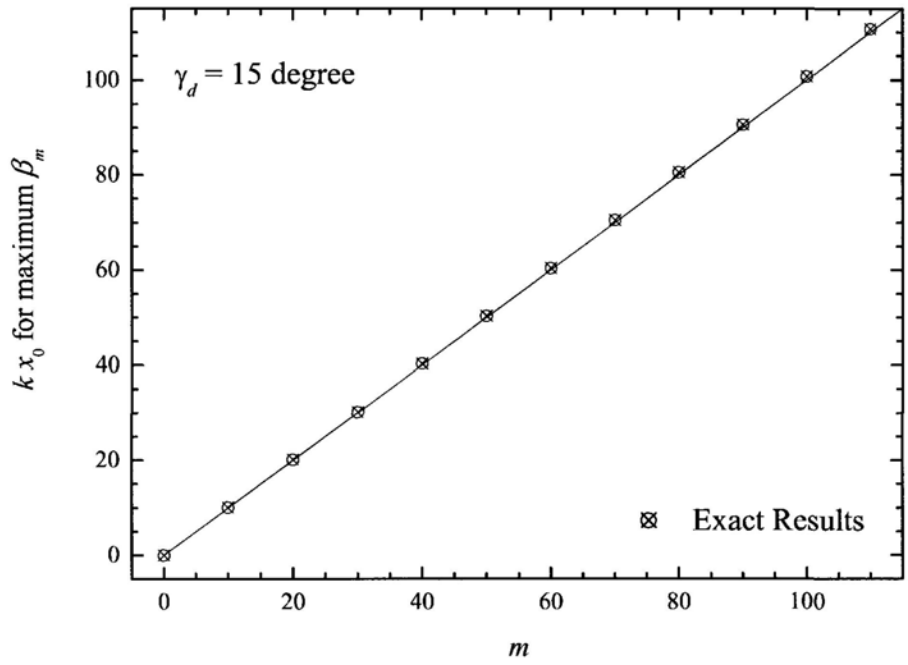

Figure 2.5: Plot of kx_0 for maximum β_m versus m, with $\gamma_d = 15°$.

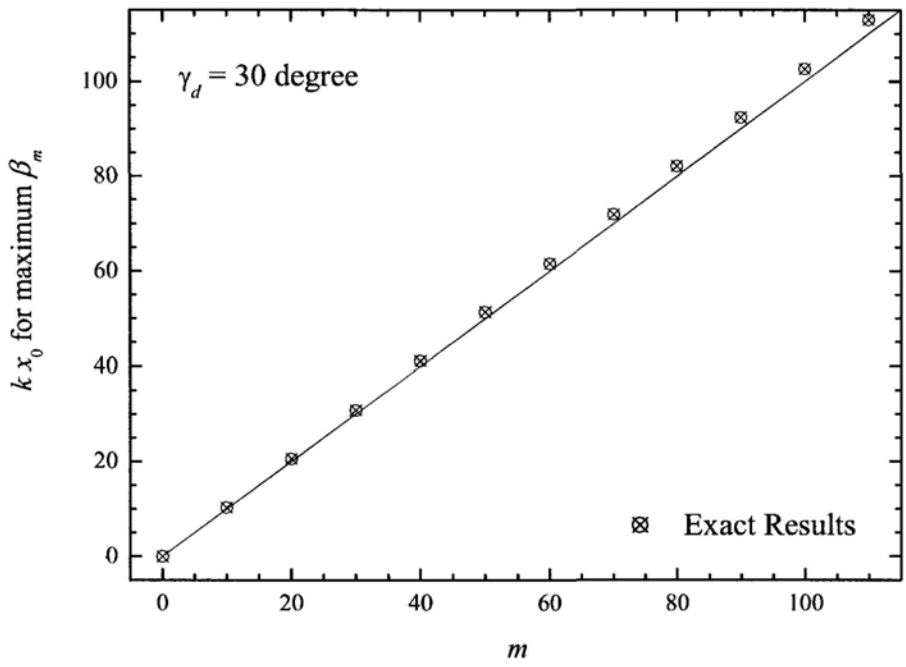

Figure 2.6: Plot of kx_0 for maximum β_m versus m, with $\gamma_d = 30°$.

2.3 Excitation of high-Q MDR's by off-surface laser beams

We have seen that the MDR of highest Q has its m close to ns so that it can be efficiently excited by a good laser beam focused at a perpendicular distance $\sim na$, which is outside the surface. There is therefore a paradox, for short wavelengths and beam waist satisfying $s \gg kw \gg 1$, that a laser beam essentially off the surface can excite an MDR of highest Q! This can be resolved from the following considerations.

First, a narrow laser beam seemingly off the surface is nevertheless touching the surface with its transverse tail. For a beam field identically zero outside a transverse range, the Fourier transform goes to zero only slowly with k_x according to the convolution theorem. This means that it can not be a laser beam of single frequency. One can even consider a field of the form $\exp[-1/(a^2-x^2)]$ for $x^2 \leq a^2$ and identically zero elsewhere. This function, the "smudge function" called by Lighthill [28], is differentiable to any order; it and all its derivatives vanish identically at $x = \pm a$. Numerical computation can easily show that its Fourier transform decreases slowly (in fact, oscillating with slowly decreasing amplitude) with k_x towards infinity. Having said that the field tail of a seemingly off-surface beam is not zero at the surface, we by no means say that the effectiveness of resonance excitation depends on the strength of the tail in the sphere. It all depends on how much the incident beam field contains the partial wave of that particular resonance, and this is precisely determined by the value of the beam-shape coefficient.

Second, since Q/s increases exponentially with s as shown in Sect. 2.1.2, the excitation of the resonance by such an off-surface laser beam necessarily

takes an exponentially long time to complete. This makes sense because the field tail of a narrow but highly collimated laser beam touching the surface could be exponentially weak. Furthermore, a huge Q/s implies a tiny line width of the resonance which could be smaller than the line width of the laser beam and, in such a case, only a small portion of the laser energy feeds the resonance.

Having discussed so, we note the experimental result of Lin et al. [29], which shows a discrepancy with the interpretation using the localization principle. Even with a rigorous derivation and thus a better understanding of the principle now, their result cannot be explained by claiming that they used a more focused beam in the experiment because such a case would predict a slightly farther impact parameter for more efficient excitation, contrary to what they have found. Seeking an explanation through the effect of surface perturbations in the literature [30, 31] is therefore well-justified.

Chapter 3

Beam-shape Coefficients and Localization Principle in Mie's scattering

Here we extend the study to the 3–D case. Both scalar wave bema and laser beams are considered.

3.1 Introduction

In the study of Mie's scattering of a laser beam incident onto a sphere either on-center or off-center, it is important to express the beam fields in terms of partial waves, each labeled by the two well-known angular momentum numbers l (principal) and m (azimuthal). The coefficient to each partial wave, symbolized by β_{lm}, say, is called the beam-shape coefficient (BSC). Obviously, the knowledge of the BSC's is crucial to the determination of the scattering characteristics. While numerical methods for the exact evaluation of such

coefficients are available, analytic approximate formulas are of course highly desirable, especially in view of the simplicity in calculation and the possible help in the conceptual understanding of the subject matter. Hence, based on the localization principle of van de Hulst [3], a localized model has been proposed and used, particularly by Gouesbet, Lock, and collaborators in their generalized Lorenz-Mie theory (GLMT) for the evaluation of the BSC [32, 33], albeit a general rigorous justification is still lacking. From their analytical work for an off-axis gaussian beam [34, 35], they conclude with a modified localized model in which the BSC is determined by the radial component of the field evaluated at a perpendicular distance of $\sqrt{(l+1/2)^2-(m+1/2)^2}/k$ from the origin in the plane perpendicular to the beam axis (i.e., the central line of the beam), where $2\pi/k$ is the wavelength and k is the wave number. This result is hardly understood physically, especially in the case of non-negligible m compared to l.

Inspired by the approximate formula for the BSC in the 2-D case for a weakly focused beam [36] and the elegant treatment of scattering of electromagnetic waves found in Jackson's text [24], we have succeeded in obtaining approximate formulas in the 3-D case with a laser beam. In particular, we show that the BSC is linearly related to the value of the transverse component of the beam field at a distance of $\sqrt{l(l+1)}/k$ from the origin in the plane perpendicular to the beam axis, irrespective of the beam position. It is essentially the coefficient of the Fourier series for the field varying along the circle of radius $\sqrt{l(l+1)}/k$ in the plane. The only assumption here is a weakly focused wave beam so that the angle of beam divergence, of the order of $1/k\sigma$, is small, where σ is a measure of the linear size of the beam waist at the focus. Our result is physically more appealing in view of the localization principle of van

de Hulst and our method is simpler than that in the GLMT. As we shall see, like that in the 2–D case, our result in fact provides a basis for and a proper understanding of the localization principle. We also want to point out that our exact expression for the BSC, being in terms of the Fourier transform of the beam field, is always independent of the radial distance (r) as it must be. This differs from that in the GLMT which relies on the choice of the beam field in the physical space; such a choice may not be an exact solution to Maxwell's equations, thus leading to r-dependent BSC. On the other hand, any choice of the Fourier transform does not have this problem.

The formulation is given in the next section. We first treat the scalar-wave case, not only because of its simplicity, but also of its real applications in scattering of sound wave beams and quantum mechanical (scalar) wave beams. We then consider the central part, the case of electromagnetic (EM) waves, of which we have particularly in mind Mie's scattering and excitation of morphology dependent resonances by focused laser beams either on-center or off-center. Because of the simplicity and elegance, Jackson's treatment is followed closely, and therefore readers are recommended to consult the relevant parts in the text. Some special field profiles, which give either exact or approximate BSC's in closed form, are considered in Section 3.3, together with comparisons. Relevance of our approximate formulas to, and thus a proper understanding of, van de Hulst's localization principle are given in Section 3.4. Discussion and conclusions are given in the last section.

3.2 Formulation

3.2.1 Scalar wave beams

Consider any single-frequency propagating scalar wave beam (e.g., a sound wave beam or a quantum mechanical scalar wave beam) satisfying the Helmholtz equation. Being finite everywhere, the beam wave field, with the time-varying factor $\exp(-i\omega t)$ omitted, can always be expanded as follows

$$\Psi(\mathbf{r}) = \sum_{lm} \beta_{lm} j_l(kr) Y_{lm}(\theta, \phi) \tag{3.1}$$

where the sum is the familiar double sum over integer l from 0 to infinity and m from $-l$ to l, $j_l(kr)$ is the spherical Bessel function of order l, $Y_{lm}(\theta, \phi)$ is the spherical harmonic of order (l, m), r, θ, and ϕ are the spherical coordinate variables, and

$$\beta_{lm} j_l(kr) = \int d\Omega \, Y^*_{lm}(\theta, \phi) \, \Psi(\mathbf{r}) \tag{3.2}$$

gives the BSC, with the integration over the entire solid angle ($d\Omega = \sin\theta d\theta d\phi$). On the other hand, the same beam wave field can have a Fourier-integral expression which is essentially a linear superposition of plane sinusoidal waves, each satisfying the same wave equation. For convenience but without loss of generality, we take the z-axis of our coordinate system parallel to the beam axis so that the expression is

$$\Psi(\mathbf{r}) = \int d^2\mathbf{k}_\perp \tilde{\Psi}(\mathbf{k}_\perp) \exp(i\mathbf{k} \cdot \mathbf{r}) \tag{3.3}$$

where the integral is over the transverse area satisfying $k_\perp \equiv \sqrt{k_x^2 + k_y^2} < k$, $d^2\mathbf{k}_\perp \equiv k_\perp dk_\perp d\phi_k$ is the area element in cylindrical coordinates, and $k_z =$

$\sqrt{k^2 - k_\perp^2} > 0$. As well-known from the expression, a cylindrically symmetric field necessarily implies a cylindrically symmetric Fourier transform, and vice versa. Note that $\tilde{\Psi}$ depends on both $\mathbf{k}_\perp$ and the position of the focus through the factor, the latter not explicitly shown in the above equation for simplicity.

Substituting Eq. (3.3) into the right-hand side of Eq. (3.2), using the following known relation

$$\exp(i\mathbf{k}\cdot\mathbf{r}) = 4\pi \sum_{lm} i^l j_l(kr) Y_{lm}^*(\theta_k, \phi_k) Y_{lm}(\theta, \phi) \tag{3.4}$$

and applying the orthonormal relations for the spherical harmonics, we readily obtain

$$\beta_{lm} = 4\pi i^l \int d^2\mathbf{k}_\perp \tilde{\Psi}(\mathbf{k}_\perp) Y_{lm}^*(\theta_k, \phi_k) \tag{3.5}$$

which, due to cancelation of the spherical Bessel function, is r-independent as it must be.

So far the expression for the BSC is exact and applies to even strongly focused beams. To find an approximate expression similar to that in the 2-D case [36], we note that $\tilde{\Psi}(\mathbf{k}_\perp)$ in Eq. (3.3) is related only to the scalar field in the xy-plane which contains essentially a Fourier series in m as obvious from (3.1). So multiplying $\Psi(\vec{r}_\perp)$ with $\exp(-im\phi)$ and integrating over the azimuthal angle, we obtain

$$\frac{1}{2\pi}\int_0^{2\pi} d\phi e^{-im\phi}\Psi(\rho, \phi, 0) = i^m \int d^2\mathbf{k}_\perp \tilde{\Psi}(\mathbf{k}_\perp) J_m(k_\perp \rho) e^{-im\phi_k} \ , \tag{3.6}$$

where the transverse position $\vec{r}_\perp$ is expressed in terms of cylindrical coordinate variables and $J_m(k_\perp\rho)$ is the (cylindrical) Bessel function of order m. We see that the left-hand side is just the m-th coefficient of the Fourier series for the

field varying along the circle of radius ρ in the xy-plane.

Furthermore, as shown in Appendix A for small angle θ, we can approximate the spherical harmonic by the Bessel function, good to first order in $\sin\theta$ and without restriction on l, according to

$$Y_{lm}(\theta,\phi) \simeq (-1)^m \sqrt{\frac{2l+1}{4\pi}} C_{lm} J_m(\sqrt{l(l+1)}\sin\theta)\, e^{im\phi} \tag{3.7}$$

Here, for convenience, we have introduced a m-symmetric coefficient defined by

$$C_{lm} \equiv \sqrt{\frac{(l+|m|)!}{[l(l+1)]^{|m|}\,(l-|m|)!}} \tag{3.8}$$

for $|m| \leq l$ and zero otherwise. Note that, for any allowed l, $C_{l,0} = C_{l,\pm 1} = 1$ and C_{lm} is monotonically decreasing with (positive) m and reaches its smallest non-zero value C_{ll}, which turns out to be very close to zero for very large l according to

$$C_{ll} \simeq (4\pi l)^{1/4}(2/e)^l \tag{3.9}$$

via the well-known Stirling approximation; for example, it is as small as 2.16×10^{-7} and 2.78×10^{-13} for $l = 50$ and $l = 100$, respectively. In passing, we note that Eq. (3.7) is essentially a relation between the associated Legendre polynomial and the Bessel functions, and we want to point out the work of MacDonald in the area. Details and our clarification are given in Appendix B. Also, for ready references, we also collect some useful formulas and relations for the Legendre polynomials and the Bessel functions in Appendix C.

For a weakly focused beam, we may take θ_k as small within the $\mathbf{k}_\perp$-integral and use the above approximation for the spherical harmonics in Eq. (3.5). The resultant integral is just of the form on the right-hand side of Eq. (3.6) if

ρ is replaced by $\sqrt{l(l+1)}/k$, $\sin\theta_k$ being equal to $k_\perp/k$. This means that the BSC, for small angle of beam divergence, is linearly determined by the field in the xy-plane at a distance of $\sqrt{l(l+1)}/k$ from the origin. More precisely, we have

$$\beta_{lm} \simeq i^{l+m}\sqrt{\frac{2l+1}{\pi}}C_{lm}\int_0^{2\pi} d\phi e^{-im\phi}\Psi(\rho,\phi,0) \tag{3.10}$$

evaluated at $\rho = \sqrt{l(l+1)}/k$. Note that the integral is basically the m-th coefficient of the Fourier series for the field varying along the circle of radius ρ in the xy-plane.

3.2.2 Electromagnetic wave beams

We now turn to the central theme. From Jackson's, the multipole expansion for the electric field ($\mathbf{E}$) and the magnetic field ($\mathbf{B}$) of any single-frequency propagating EM wave beam, omitting the time-varying factor, takes the following general form

$$\mathbf{E}(\mathbf{r}) = \sum_{lm}\left[\beta_M(lm)j_l(kr)\mathbf{X}_{lm} + (i/k)\beta_E(lm)\nabla\times j_l(kr)\mathbf{X}_{lm}\right], \tag{3.11}$$

and

$$c\mathbf{B}(\mathbf{r}) = \sum_{lm}\left[\beta_E(lm)j_l(kr)\mathbf{X}_{lm} - (i/k)\beta_M(lm)\nabla\times j_l(kr)\mathbf{X}_{lm}\right], \tag{3.12}$$

respectively, where the double sum is the same as that in Eq. (3.1) except l is now from 1 to infinity, $\mathbf{X}_{lm}$ is the vector spherical harmonic of order (l,m), and $\beta_M(lm)$ [$\beta_E(lm)$] is the BSC for the so-called magnetic [electric] multipole wave, which is also called the transverse electric [magnetic] wave or simply

the TE [TM] wave in view of the field direction with respect to the position vector. Taking the inner product with the complex conjugate of the vector spherical harmonic, integrating over the entire solid angle, and making use of the orthonormal relations, we have

$$\beta_M(lm)j_l(kr) = \int d\Omega\, \mathbf{X}^*_{lm} \cdot \mathbf{E}(\mathbf{r}) \tag{3.13}$$

and

$$\beta_E(lm)j_l(kr) = c\int d\Omega\, \mathbf{X}^*_{lm} \cdot \mathbf{B}(\mathbf{r}) \tag{3.14}$$

Like the scalar-wave case, another integral expression for the fields exists. To keep our treatment somewhat parallel to Jackson's for the convenience of later-on calculations, we choose to express the above electric field, and similarly for the magnetic field, as

$$\mathbf{E}(\mathbf{r}) = \mathbf{E}^{(+)}(\mathbf{r}) + \mathbf{E}^{(-)}(\mathbf{r}) \tag{3.15}$$

with

$$\mathbf{E}^{(\pm)}(\mathbf{r}) = \int d^2\mathbf{k}_\perp \tilde{E}^{(\pm)}(\mathbf{k}_\perp)\left(\mathbf{e}_x \pm i\mathbf{e}_y - \frac{k_x \pm ik_y}{k_z}\mathbf{e}_z\right)\exp(i\mathbf{k}\cdot\mathbf{r}), \tag{3.16}$$

where we have again chosen the z-axis parallel to the beam axis. (Note again that $\tilde{E}^{(\pm)}$ depends on both $\mathbf{k}_\perp$ and the position of the focus, the latter not explicitly shown in the above equation for simplicity.) We may call $\mathbf{E}^{(+)}$ and $\mathbf{E}^{(-)}$ the right-hand and left-hand rotating (in the transverse plane) fields, respectively, and a field of any other state can be obtained from an appropriate combination of them. Obviously, each field in Eq. (3.16) is an exact solution of Maxwell's equations. Hence, each has a multipole expansion like that in Eq.

(3.11) with its corresponding BSC's, on which we shall henceforth concentrate without loss of generality. Now by substituting the above integral for $\mathbf{E}^{(\pm)}$ into Eq. (3.13), repeating essentially Jackson's steps in obtaining the multipole expansions for circularly polarized plane wave fields, and following the steps leading to Eq. (3.5), we obtain

$$\beta_M^{(\pm)}(lm) = 4\pi i^l \int d^2\mathbf{k}_\perp \frac{\tilde{E}^{(\pm)}(\mathbf{k}_\perp)}{\sqrt{l(l+1)}} \left[\sqrt{(l \pm m)(l \mp m + 1)} Y^*_{l,m\mp 1}(\Omega_k) - m e^{\pm i\phi_k} \tan\theta_k Y^*_{lm}(\Omega_k)\right] \quad (3.17)$$

where we have in fact used the definition $\mathbf{X}_{lm} \equiv \mathbf{L}Y_{lm}/\sqrt{l(l+1)}$ with $\mathbf{X}_{lm} \equiv 0$ for $l = 0$, and the following relations involving the angular momentum operator $\mathbf{L}$: $\mathbf{L} \cdot (\mathbf{e}_x \pm i\mathbf{e}_y) = \mathrm{L}_\pm$, $\mathrm{L}_\pm Y_{lm} = \sqrt{(l \mp m)(l \pm m + 1)} Y_{l,m\pm 1}$, and $\mathrm{L}_z Y_{lm} = mY_{lm}$, and Ω_k indicates the dependence of the spherical harmonics on the two angles θ_k and ϕ_k in the $\mathbf{k}$-space. Note that the appearance of $Y_{l,l+1}$ and $Y_{l,-l-1}$ should not be a problem because their respective preceding factors vanish in such cases.

Equation (3.17) is an exact expression for the BSC and it is r-independent as it must be. It is expressed in terms of the Fourier transform of the beam field rather than the beam field itself, and any choice of the Fourier transform is compatible with Maxwell's equations. It applies for any rotating (in the transverse plane) wave field no matter how the beam is focused. Of course, any other state of wave can be obtained from Eq. (3.15). For example, a wave field with transverse component only along the x-direction [y-direction] can be obtained by taking $\tilde{E}^{(-)} = \tilde{E}^{(+)}$ [$\tilde{E}^{(-)} = -\tilde{E}^{(+)}$] in Eq. (3.16) and the subsequent BSC in Eq. (3.13) is given by $\beta_M^{(x)}(lm) = \beta_M^{(+)}(lm) + \beta_M^{(-)}(lm)$

$[\beta_M^{(y)}(lm) = \beta_M^{(+)}(lm) - \beta_M^{(-)}(lm)]$. In a similar fashion, the BSC for the electric multipole (TM) waves can be obtained via the integral form for the wave magnetic wave expressed like that in Eq. (3.16). The derivation is straightforward and we simply give the result below

$$\begin{aligned}\beta_E^{(\pm)}(lm) = \mp 4\pi i^{l+1} \int d^2\mathbf{k}_\perp \frac{\tilde{E}^{(\pm)} \cos\theta_k}{\sqrt{l(l+1)}} \\ \Big\{ \sqrt{(l \pm m)(l \mp m + 1)} Y^*_{l,m\mp 1} - m \tan\theta_k e^{\pm i\phi_k} Y^*_{lm} \\ \mp \frac{\tan^2\theta_k}{2} e^{\pm i\phi_k} \Big[\sqrt{(l-m)(l+m+1)} Y^*_{l,m+1} e^{i\phi_k} \\ - \sqrt{(l+m)(l-m+1)} Y^*_{l,m-1} e^{-i\phi_k} \Big] \Big\} \end{aligned} \quad (3.18)$$

Naturally, the two exact expressions can be used for numerical evaluations of the BSC's if the Fourier transforms of the fields are known. There is no worry of the r-dependence.

We now want to approximate the expression in a way similar to the scalar-wave case. Here $\tilde{E}^{(\pm)}(\mathbf{k}_\perp)$ is related only to the transverse component of the electric field in Eq. (3.16) in the xy-plane which, when multiplied with $\exp(-im\phi)$ and after integration over the azimuthal angle, leads exactly to

$$\mathcal{E}_m^{(\pm)}(\rho) = i^m \int d^2\mathbf{k}_\perp \tilde{E}^{(\pm)}(\mathbf{k}_\perp) J_m(k_\perp \rho) e^{-im\phi_k} \quad (3.19)$$

where

$$\mathcal{E}_m^{(\pm)}(\rho) \equiv \frac{1}{2\pi} \int_0^{2\pi} d\phi e^{-im\phi} E_\perp^{(\pm)}(\rho, \phi) \ , \quad (3.20)$$

is the m-th coefficient of the Fourier series for the transverse field varying along the circle of radius ρ in the xy-plane.

For a laser beam of small angle of divergence, we can readily apply the

approximation Eq. (3.7) for the evaluation of the first integral in Eq. (3.17) and, via Eq. (3.19), obtain the dominant part

$$\beta_{M0}^{(\pm)}(lm) = 2\sqrt{\pi} i^{l+m\mp 1} \sqrt{\frac{(2l+1)(l\pm m)(l\mp m+1)}{l(l+1)}} C_{l,m\mp 1} \mathcal{E}_{m\mp 1}^{(\pm)}(\rho) \quad (3.21)$$

evaluated at $\rho = \sqrt{l(l+1)}/k$, where $\beta_{M0}^{(+)}(l,-l) = \beta_{M0}^{(-)}(l,l) = 0$ should be noted. The second integral, which is first order in $\sin\theta_k \simeq \tan\theta_k$ for small θ_k, can be obtained for $\beta_M^{(+)}$ and $\beta_M^{(-)}$ separately in a similar way via the following general relations [37, 38]

$$\begin{aligned}(2l+1)\sin\theta\, P_l^m(\cos\theta) &= P_{l-1}^{m+1}(\cos\theta) - P_{l+1}^{m+1}(\cos\theta) \\ &= (l-m+2)(l-m+1)P_{l+1}^{m-1}(\cos\theta) - (l+m)(l+m-1)P_{l-1}^{m-1}(\cos\theta)\end{aligned} \quad (3.22)$$

and Eq. (3.7). The derivation is straight-forward and the subdominant BSC turns out to be

$$\begin{aligned}\beta_{M1}^{(\pm)}(lm) = \frac{2\sqrt{\pi} i^{l+m+1} m}{\sqrt{l(l+1)(2l+1)}} \Big[&\sqrt{(l\mp m+2)(l\mp m+1)} C_{l+1,m\mp 1} \mathcal{E}_{m\mp 1}^{(\pm)}(\rho_b) \\ &- \sqrt{(l\pm m)(l\pm m-1)} C_{l-1,m\mp 1} \mathcal{E}_{m\mp 1}^{(\pm)}(\rho_s) \Big]\end{aligned} \quad (3.23)$$

where $\rho_b \equiv \sqrt{(l+1)(l+2)}/k$ is a bigger radius and $\rho_s \equiv \sqrt{(l-1)l}/k$ is a smaller radius, when compared with the radius $\sqrt{l(l+1)}/k$, and we should also note that the second term vanishes for $m = \mp l$. Since the field varies on the scale σ, which is much larger than the difference in radius, we may simplify the result via the following expansions without loss of precision within our

approximation

$$\mathcal{E}_m^{(\pm)}(\rho_b) \simeq \mathcal{E}_m^{(\pm)}(\rho) + \frac{\sqrt{(l+1)(l+2)} - \sqrt{l(l+1)}}{k} \frac{d\mathcal{E}_m^{(\pm)}(\rho)}{d\rho} \tag{3.24}$$

and

$$\mathcal{E}_m^{(\pm)}(\rho_s) \simeq \mathcal{E}_m^{(\pm)}(\rho) - \frac{\sqrt{l(l+1)} - \sqrt{(l-1)l}}{k} \frac{d\mathcal{E}_m^{(\pm)}(\rho)}{d\rho} \tag{3.25}$$

all evaluated at $\rho = \sqrt{l(l+1)}/k$; the second term being smaller by an order of $1/k\sigma$ is obvious. From Eq. (3.18) and under the same approximation, the BSC for the electric multipole (TM) wave can be shown to be simply given by

$$\beta_E^{(\pm)}(lm) = \mp i\beta_M^{(\pm)}(lm) \tag{3.26}$$

Note that the derivation does not require the knowledge of the exact form of the beam field and thus our results apply to a beam of any shape so long as we have a small angle of beam divergence.

3.3 Explicit BSC's for some special cases

3.3.1 Exact results for beams of cylindrical symmetry

For beams of cylindrical symmetry, the beam field and thus its Fourier transform are independent of the azimuthal angle and the beam axis must pass through the origin. Under this condition, Eq. (3.5) for the scalar-wave case and Eq. (3.17) for the EM-wave case can be simplified to

$$\beta_{lm} = 4\pi i^l \sqrt{\pi(2l+1)} \int_0^k k_\perp dk_\perp \tilde{\Psi}(k_\perp) P_l(\cos\theta_k)\ \delta_{m,0} \tag{3.27}$$

and

$$\beta_M^{(\pm)}(lm) = 4\pi i^l \sqrt{\pi(2l+1)} \int_0^k k_\perp dk_\perp \tilde{E}^{(\pm)}(k_\perp) \left[P_l(\cos\theta_k) - \frac{\tan\theta_k}{l(l+1)} \frac{dP_l(\cos\theta_k)}{d\theta_k} \right] \delta_{m,\pm 1} \quad (3.28)$$

respectively.

With these preliminaries, we consider a plane wave as a first example. The field is a constant, taken to be unity for simplicity, so that its Fourier transform is given by $\delta(k_\perp)/2\pi k_\perp$, a 2-dimensional Dirac delta function with cylindrical symmetry. Hence, the above two equations readily reduce to

$$\beta_{lm} = i^l \sqrt{4\pi(2l+1)}\, \delta_{m,0} \quad (3.29)$$

and

$$\beta_M^{(\pm)}(l,m) = i^l \sqrt{4\pi(2l+1)}\, \delta_{m,\pm 1}\ , \quad (3.30)$$

respectively, the latter being exactly the result obtained by Jackson. Note that they can also be obtained from Eq. (3.10) and Eq. (3.21) because $\sin\theta_k$ is zero exactly.

As a second example, we take the Fourier transformed field to be a constant within a certain circle in the $\mathbf{k}_\perp$-plane, i.e.,

$$\tilde{\Psi}(\mathbf{k}_\perp) = \tilde{E}^{(\pm)}(\mathbf{k}_\perp) = 1/\pi k_d^2 \qquad \text{for} \qquad k_\perp \leq k_d < k \quad (3.31)$$

and zero otherwise, where we have chosen the constant to be such that the

corresponding wave field in the xy-plane, readily given by

$$\Psi(\rho, \phi, 0) = E_{\perp}^{(\pm)}(\rho, \phi) = 2J_1(k_d\rho)/k_d\rho \ , \tag{3.32}$$

approaches unity at the origin. In passing, we note that, in the limit of zero k_d, the Fourier transformed becomes a Dirac delta function and the wave field itself becomes a constant, implying the plane-wave case.

The only non-zero BSC for the scalar-wave case can then be obtained directly from Eq. (3.27) by carrying out the integration [39]. The result is

$$\beta_{l0} = \frac{4i^l k^2}{k_d^2} \frac{\sqrt{\pi(2l+1)}}{l+2} \left[\frac{l \cos\theta_d P_{l-1}(\cos\theta_d) - P_l(\cos\theta_d)}{l-1} - \cos^2\theta_d P_l(\cos\theta_d) \right] \tag{3.33}$$

where

$$\theta_d = \sin^{-1}(k_d/k) \ < \ \pi/2 \tag{3.34}$$

is obviously the angle of beam divergence. For convenience, we give, for $l = 1$

$$\beta_{1,0} = \frac{4ik^2}{k_d^2} \sqrt{\frac{\pi}{3}} (1 - \cos^3\theta_d) \tag{3.35}$$

In a similar way, the only non-zero BSC's for the EM-wave case can be obtained directly from Eq. (3.28) to be

$$\beta_M^{(\pm)}(l, \pm 1) = \beta_{l0} - \frac{4i^l k^2}{k_d^2} \frac{\sqrt{\pi(2l+1)}}{(l+1)(l+2)} \times \left[\sin^2\theta_d \ P_l(\cos\theta_d) + 2 \ \frac{P_l(\cos\theta_d) - \cos\theta_d P_{l-1}(\cos\theta_d)}{l-1} \right] \tag{3.36}$$

and, for convenience, we give

$$\beta_M^{(\pm)}(1,\pm 1) = \beta_{1,0} + \frac{4ik^2}{k_d^2}\sqrt{\frac{\pi}{3}}\,\frac{(2+\cos\theta_d)(1-\cos\theta_d)^2}{2} \tag{3.37}$$

for $l = 1$. Note that the first term, which is the same as that in the scalar-wave case, comes from the first integral in Eq. (3.17); it dominates for small θ_d as expected, yet it becomes comparable to the second term otherwise. Note also that we have the plane-wave case in the limit of zero θ_d, and the results in Eq. (3.29) and Eq. (3.30) are recovered from Eq. (3.33) and Eq. (3.36), respectively.

3.3.2 Approximate results for gaussian beams

Consider a gaussian beam weakly focused on the x-axis at a distance ρ_0 from the origin. We may therefore take

$$\Psi(\rho,\phi,0) = E_\perp^{(\pm)}(\rho,\phi) = \exp\left(-\frac{\rho^2 - 2\rho\rho_0\cos\phi + \rho_0^2}{2\sigma^2}\right) \tag{3.38}$$

so that the integral in Eq. (3.10) and those for the Fourier-series coefficients in Eq. (3.21) and Eq. (3.23) can be performed to yield modified Bessel functions. For the scalar-wave case, the result is

$$\beta_{lm} = i^{l+m}\sqrt{4\pi(2l+1)}C_{lm}\exp\left(-\frac{\rho^2+\rho_0^2}{2\sigma^2}\right) I_m(\rho\rho_0/\sigma^2) \tag{3.39}$$

evaluated at $\rho = \sqrt{l(l+1)}/k$. For the electromagnetic-wave case, the dominant result is

$$\beta_{M0}^{(\pm)}(lm) = i^{l+m\mp1}\sqrt{\frac{4\pi(2l+1)(l\pm m)(l\mp m+1)}{l(l+1)}} \\ C_{l,m\mp1}\exp(-\frac{\rho^2+\rho_0^2}{2\sigma^2})I_{m\mp1}(\rho\rho_0/\sigma^2) \quad (3.40)$$

evaluated at $\rho = \sqrt{l(l+1)}/k$, while the subdominant result is

$$\beta_{M1}^{(\pm)}(lm) = \frac{\sqrt{4\pi}i^{l+m+1}m}{\sqrt{l(l+1)(2l+1)}} \\ \left[\sqrt{(l\mp m+2)(l\mp m+1)}C_{l+1,m\mp1}\exp(-\frac{\rho_b^2+\rho_0^2}{2\sigma^2})I_{m\mp1}(\frac{\rho_b\rho_0}{\sigma^2})\right. \\ \left.-\sqrt{(l\pm m)(l\pm m-1)}C_{l-1,m\mp1}\exp(-\frac{\rho_s^2+\rho_0^2}{2\sigma^2})I_{m\mp1}(\frac{\rho_s\rho_0}{\sigma^2})\right] \quad (3.41)$$

Expectedly, Eq. (3.39) and Eq. (3.40) reduce to Eq. (3.29) and Eq. (3.30) respectively in the limit of infinite σ (i.e., the plane-wave case), the subdominant result being zero. Furthermore, for the beam focused at the origin so that $\rho_0 = 0$, we have, for the scalar-wave case,

$$\beta_{lm} = i^l\sqrt{4\pi(2l+1)}\exp\left(-\frac{l(l+1)}{2k^2\sigma^2}\right)\delta_{m,0} \quad (3.42)$$

and, for the electromagnetic-wave case, the dominant result is

$$\beta_{M0}^{(\pm)}(lm) = i^l\sqrt{4\pi(2l+1)}\exp\left(-\frac{l(l+1)}{2k^2\sigma^2}\right)\delta_{m,\pm1} \quad (3.43)$$

while the subdominant result takes the following form via the expansion similar to Eq. (3.24) and Eq. (3.25)

$$\beta_{M1}^{(\pm)}(lm) = i^l \sqrt{\frac{4\pi l(l+1)}{2l+1}} \frac{\sqrt{(l+1)(l+2)} - \sqrt{(l-1)l}}{k^2\sigma^2} \exp\left(-\frac{l(l+1)}{2k^2\sigma^2}\right) \delta_{m,\pm 1} \tag{3.44}$$

which may be ignored in our approximation.

3.3.3 A comparison of results

As a check of the approximation, we compare Eq. (3.33), the exact BSC expression for the scalar-wave beam modeled by Eq. (3.31), with the following approximate expression

$$\beta_{l0} = 4i^l \sqrt{\pi(2l+1)} \frac{J_1\left(\sqrt{l(l+1)}k_d/k\right)}{\sqrt{l(l+1)}k_d/k} \tag{3.45}$$

according to Eq. (3.10), where the wave function in Eq. (3.32) has been substituted. Noticing that the two give exactly the same constant value (in fact, $2\sqrt{\pi}$) for $l = 0$, we plot in Fig. 3.1 the BSC values versus θ_d (in degrees), the (half) angle of beam divergence, for $l = 1$, 5, 25 and 100 as examples, the solid lines giving the exact results and the dashed lines the approximate results. As we can see, the comparison is very satisfactory. The two lines for each l, while different slightly for large θ_d, are completely indistinguishable for small θ_d, as expected.

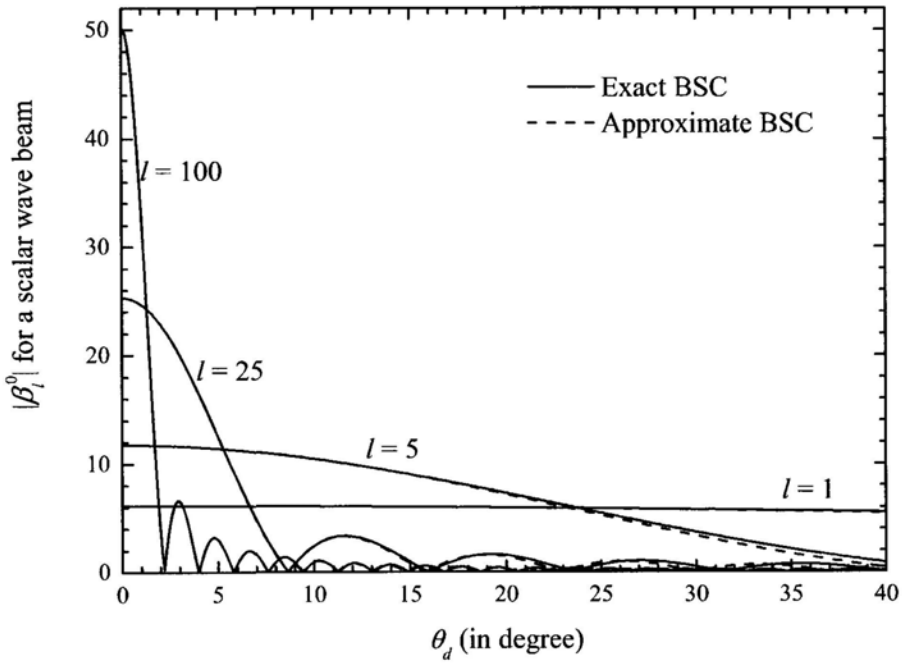

Figure 3.1: Comparison of the exact BSC for the scalar-wave beam modeled by Eq. (3.31) with the approximate BSC according to Eq. (3.45) for $l = 1$, 5, 25 and 100.

3.4 Relevance to the localization principle of van de Hulst

Like that in the 2–D case, there is a question of the statement by van de Hulst regarding the localization principle, namely, a term of order l is a widespread wave, and so how can it correspond to a localized ray? It turns out that our approximate BSC, derived from first principle, can answer this question and thus provides a proper perspective of the principle, in a somewhat similar way, as in the 2–D case.

A ray is meaningful only in geometric optics, just like that a localized electron is a semi-classical concept. From the viewpoint of wave optics, it is really like a highly collimated gaussian beam of waist size much greater than the wavelength, i.e., $k\sigma >>> 1$. As such, the BSC's for the beam electric and magnetic fields, which are respectively given by Eq. (3.11) and Eq. (3.12), are well-approximated by the expressions in Eq. (3.21) [or Eq. (3.40) in case of a gaussian beam] and Eq. (3.26), or their linear combinations depending on the state of wave polarization (in the transverse plane). If the beam axis is at a distance of ρ_0 from the origin satisfying $\rho_0 \gg \sigma$, the beam field is essentially zero outside the radius range $(\rho_0 - \sigma, \rho_0 + \sigma)$; our results immediately show that we can safely neglect those BSC's with angular momentum number l lying outside the range $(k\rho_0 - k\sigma, k\rho_0 + k\sigma)$. This means that the summation over the angular momentum number in Eq. (3.11) and Eq. (3.12) for the beam fields need only cover those l's in the range and there are many such numbers around the average angular momentum number, $\bar{l}$, say. So, it is not that one term of order l corresponds to the ray but really that *many terms of neighboring l's around the average $\bar{l}$ corresponds to the ray passing the center*

at a distance $\bar{l}/k$, noting that $\sqrt{l(l+1)} \simeq l + 1/2 \simeq l$ for large l. With this understanding, one can repeat the elegant work of van de Hulst on the scattering of a ray by a large sphere in expanding the scattering coefficient of one angular momentum number into a series of terms, the first giving rise to the immediate reflected ray, and the rest giving rise to the subsequent refracted rays. But here again many neighboring angular momentum numbers are involved, yet the conclusion is the same if his angular momentum number is replaced by the average $\bar{l}$; this is so because the scattering coefficient is a smooth function of the angular momentum number for the case of beams hitting the sphere. In this connection, we would like to point out that the latter smoothness breaks down for morphology-dependent resonances (MDR's) of high-quality (Q) factor, yet fortunately such high-Q MDR's occur for l lying between the size parameter ka and nka (n the refractive index and a the radius of the sphere) which corresponds to beams passing just off the sphere.

3.5 Discussion and conclusions

We have obtained exact and r-independent expressions [i.e., Eq. (3.5), Eq. (3.17) and Eq. (3.18)] for beam-shape coefficients (BSC) of order lm in the partial-wave expansion of any wave beam field in various cases. From them we have derived, for weakly focused beams or well-collimated beams, approximate expressions [i.e., Eq. (3.10), Eq. (3.21) and Eq. (3.23), and Eq. (3.26)] which are linearly related to the value of the beam field at a transverse distance of $\sqrt{l(l+1)}/k$ from the origin, the latter being recognized as the expectation value of the angular momentum divided by the linear momentum of a electron

wave beam in the semi-classical regime of quantum mechanics. Explicit BSC's in closed form for a number of cases have been found, and comparisons of exact and approximate results made to show how good the approximation is. The relevance of our approximation to van de Hulst's localization principle has been shown; this helps to put the principle in a proper prospective as regards conceptual understanding.

The BSC's for a wave beam is irrespective of the existence of a scatterer, yet its usefulness relies very much on it. This is particularly so for a sphere at the origin by which an on-center, off-center or even off-sphere wave beams are being scattered and high-Q MDR's are excited. We hope to come back to such problems in the near future.

Appendix A

$P_l^m(\cos\theta)$ Approximated by $J_m(\sqrt{l(l+1)}\sin\theta)$ for Small θ — Our Approximation

Consider the differential equation for the associated Legendre function

$$\left[\frac{1}{\sin\theta}\frac{d}{d\theta}\sin\theta\frac{d}{d\theta}+l(l+1)-\frac{m^2}{\sin^2\theta}\right]P_l^m(\cos\theta)=0 \qquad \text{(A.1)}$$

If we change the variable θ to $\xi \equiv \sqrt{l(l+1)}\sin\theta$, it becomes

$$\left[(1-\sin^2\theta)\frac{d^2}{d\xi^2}+(1-2\sin^2\theta)\frac{d}{\xi d\xi}+1-\frac{m^2}{\xi^2}\right]P_l^m(\cos\theta)=0 \qquad \text{(A.2)}$$

for $0 \leq \theta \leq \pi/2$. Assuming small θ so that $\sin^2\theta$ can be ignored compared to unity, the above equation immediately reduces to the well-known Bessel differential equation with the solution $J_m(\xi)$. This means that $P_l^m(\cos\theta)$ is linearly related to $J_m(\sqrt{l(l+1)}\sin\theta)$. The proportionality constant can be determined

by comparing the appropriate series expansions for the two functions. It turns out that it is easier to find the following relation for $m \leq 0$

$$P_l^m(\cos\theta) \simeq \left[-\sqrt{l(l+1)}\right]^m J_m(\sqrt{l(l+1)}\sin\theta) \ , \tag{A.3}$$

from which we can easily obtain, for $m \geq 0$,

$$P_l^m(\cos\theta) \simeq \frac{(l+m)!}{(l-m)!}\left[-\sqrt{l(l+1)}\right]^{-m} J_m(\sqrt{l(l+1)}\sin\theta) \tag{A.4}$$

via

$$P_l^m(\cos\theta) = (-1)^m \frac{(l+m)!}{(l-m)!} P_l^{-m}(\cos\theta) \ , \tag{A.5}$$

an exact relation. Now Eq. (3.7) can be obtained by using the definition

$$Y_{lm}(\Omega) \equiv \sqrt{\frac{2l+1}{4\pi}\frac{(l-m)!}{(l+m)!}} P_l^m(\cos\theta)\, e^{im\phi} \tag{A.6}$$

without much difficulty. Note that our derivation requires neither $l \gg 1$ nor $l\sin\theta < 1$. This is different from the MacDonald approximation as understood in the literature [40, 41].

Appendix B

The Relation between Legendre Functions and Bessel Functions — Generalized MacDonald Approximation

B.1 Background

MacDonald [42–44] obtained an approximate expression for an arbitrary associated Legendre function in terms of Bessel functions. While MacDonald did not specify the limitation on l, The prevailing view is that this approximation is applicable for $l \gg 1$ [45, 9.722 on pp. 963] and [41]. However, it is shown in this section that the approximation is also applicable for small l, such as $l = 0, 1, 2, \cdots$. With such an understanding, we can use MacDonald approximation when considering on-center or near-center cases, in which the indices l are not so large.

B.2 Analytical Derivation

From the general form of associated Legendre functions, suggested by I. S. Gradshteyn and I. M. Ryzhik [45, Eq. (8.704) on pp. 959], we obtain that

$$\begin{aligned} P_l^{-m}(\cos\theta) &= \frac{1}{\Gamma(1+m)}\left[\frac{1-\cos\theta}{1+\cos\theta}\right]^{\frac{m}{2}} F\left(-l, l+1; 1+m; \frac{1-\cos\theta}{2}\right) \\ &= \left[\frac{1-\cos\theta}{1+\cos\theta}\right]^{\frac{m}{2}} \sum_{r=0}^{\infty} \frac{\Gamma(r-l)\Gamma(r+l+1)}{\Gamma(-l)\Gamma(l+1)\Gamma(r+m+1)\Gamma(r+1)} \left(\frac{1-\cos\theta}{2}\right)^r \\ &= \left[\frac{1-\cos\theta}{1+\cos\theta}\right]^{\frac{m}{2}} \sum_{r=0}^{\infty} \frac{\Gamma(l+r+1)}{\Gamma(l-r+1)} \frac{(-)^r}{\Gamma(r+m+1)\Gamma(r+1)} \left(\frac{1-\cos\theta}{2}\right)^r, \end{aligned} \tag{B.1}$$

where the indices l, m lying on the interval $[-l, +l]$, are both integers, and the angle θ is a real number, so that the argument $\cos\theta$ lies on the interval $[-1, +1]$. Note that the normalization factor is slightly different from $(-)^{m/2}$, suggested by M. Abramowitz and I. A. Stegun [46, Eq. (8.1.2)], which is also widely used.

For arbitrary positive integer $l \geq r > 1$, we expand the polynomial as

$$\begin{aligned} \frac{\Gamma(l+r+1)}{\Gamma(l-r+1)} &= (l-r+1)(l-r+2)\cdots l(l+1)\cdots(l+r-1)(l+r) \\ &= \left[\left(l+\frac{1}{2}\right) - \left(r-\frac{1}{2}\right)\right]\left[\left(l+\frac{1}{2}\right) - \left(r-\frac{3}{2}\right)\right]\cdots\left[\left(l+\frac{1}{2}\right) - \frac{1}{2}\right] \\ &\quad \left[\left(l+\frac{1}{2}\right) + \frac{1}{2}\right]\cdots\left[\left(l+\frac{1}{2}\right) + \left(r-\frac{3}{2}\right)\right]\left[\left(l+\frac{1}{2}\right) + \left(r-\frac{1}{2}\right)\right] \\ &= \left[\left(l+\frac{1}{2}\right)^2 - \left(r-\frac{1}{2}\right)^2\right]\left[\left(l+\frac{1}{2}\right)^2 - \left(r-\frac{3}{2}\right)^2\right]\cdots \\ &\quad \cdots\left[\left(l+\frac{1}{2}\right)^2 - \left(1-\frac{1}{2}\right)^2\right] \\ &= \left(l+\frac{1}{2}\right)^{2r} + A\left(l+\frac{1}{2}\right)^{2r-2} + B\left(l+\frac{1}{2}\right)^{2r-4} + \cdots + C, \end{aligned} \tag{B.2}$$

and the coefficients

$$A = -\sum_{i=1}^{r}\left(i-\frac{1}{2}\right)^2 = -\frac{r(2r-1)(2r+1)}{12}$$
$$= -\frac{1}{3}\frac{\Gamma(r+1)}{\Gamma(r-2)} - \frac{\Gamma(r+1)}{\Gamma(r-1)} - \frac{1}{4}\frac{\Gamma(r+1)}{\Gamma(r)}, \quad \text{(B.3)}$$

$$B = \sum_{i=1}^{r-1}\sum_{j=i+1}^{r}\left(i-\frac{1}{2}\right)^2\left(j-\frac{1}{2}\right)^2$$
$$= \frac{r(r-1)(2r-3)(2r-1)(2r+1)(10r+7)}{1440}$$
$$= \frac{1}{18}\frac{\Gamma(r+1)}{\Gamma(r-5)} + \frac{11}{15}\frac{\Gamma(r+1)}{\Gamma(r-4)}$$
$$+ \frac{31}{12}\frac{\Gamma(r+1)}{\Gamma(r-3)} + \frac{29}{12}\frac{\Gamma(r+1)}{\Gamma(r-2)} + \frac{9}{32}\frac{\Gamma(r+1)}{\Gamma(r-1)}. \quad \text{(B.4)}$$

For $l \geq r = 1$,

$$\frac{\Gamma(l+r+1)}{\Gamma(l-r+1)} = l(l+1) = \left(l+\frac{1}{2}\right)^2 - \frac{1}{4}. \quad \text{(B.5)}$$

For $l \geq r = 0$,

$$\frac{\Gamma(l+r+1)}{\Gamma(l-r+1)} = 1 = \left(l+\frac{1}{2}\right)^0. \quad \text{(B.6)}$$

For $r > l \geq 0$,

$$\frac{\Gamma(l+r+1)}{\Gamma(l-r+1)} = 0. \quad \text{(B.7)}$$

We obtain that

$$P_l^{-m}(\cos\theta) = \left[\frac{1-\cos\theta}{1+\cos\theta}\right]^{\frac{m}{2}}$$
$$\sum_{r=0}^{l}\frac{\Gamma(l+r+1)}{\Gamma(l-r+1)}\frac{(-)^r}{\Gamma(r+m+1)\Gamma(r+1)}\left(\frac{1-\cos\theta}{2}\right)^r$$

$$\approx \left[\frac{1-\cos\theta}{1+\cos\theta}\right]^{\frac{m}{2}} \sum_{r=0}^{l} \frac{(-)^r \left(l+\frac{1}{2}\right)^{2r}}{\Gamma(r+m+1)\Gamma(r+1)} \left(\frac{1-\cos\theta}{2}\right)^r$$
$$+ \left[\frac{1-\cos\theta}{1+\cos\theta}\right]^{\frac{m}{2}} \sum_{r=1}^{l} \frac{(-)^r A\left(l+\frac{1}{2}\right)^{2r-2}}{\Gamma(r+m+1)\Gamma(r+1)} \left(\frac{1-\cos\theta}{2}\right)^r$$
$$+ \left[\frac{1-\cos\theta}{1+\cos\theta}\right]^{\frac{m}{2}} \sum_{r=2}^{l} \frac{(-)^r B\left(l+\frac{1}{2}\right)^{2r-4}}{\Gamma(r+m+1)\Gamma(r+1)} \left(\frac{1-\cos\theta}{2}\right)^r, \quad \text{(B.8)}$$

where we have ignored the terms of order $\left(n+\frac{1}{2}\right)^{2r-6}$, $\left(n+\frac{1}{2}\right)^{2r-8}$, etc. Numerical simulation will be delivered in the following context to check the validity of the truncation.

Comparing Eq. (B.8) with Eq. (9.1.10) of M. Abramowitz and I. A. Stegun [46]. the ascending series of Bessel functions of the first kind (of integer order)

$$J_m(x) = \left(\frac{x}{2}\right)^m \sum_{r=0}^{\infty} (-)^r \frac{(x/2)^{2r}}{\Gamma(r+m+1)\Gamma(r+1)}, \quad \text{(B.9)}$$

we finally obtain the MacDonald approximation

$$P_l^{-m}(\cos\theta) \approx \left[\left(l+\frac{1}{2}\right)\cos\frac{\theta}{2}\right]^{-m} \left\{J_m(\mu) + \sin^2\frac{\theta}{2}\left[\frac{\mu}{6}J_{m+3}(\mu) - J_{m+2}(\mu) + \frac{1}{2\mu}J_{m+1}(\mu)\right]\right\}, \quad \text{(B.10a)}$$

and

$$P_l^{m}(\cos\theta) \approx \left[-\left(l+\frac{1}{2}\right)\cos\frac{\theta}{2}\right]^{m} \left\{J_m(\mu) - \sin^2\frac{\theta}{2}\left[\frac{\mu}{6}J_{m-3}(\mu) + J_{m-2}(\mu) + \frac{1}{2\mu}J_{m-1}(\mu)\right]\right\}, \quad \text{(B.10b)}$$

when the parameter $\mu = (2l+1)\sin\frac{\theta}{2}$ is neither too large nor too small.

When $m = 0$, the formula can be further reduced to

$$P_l(\cos\theta) \approx \left\{ J_0(\mu) + \sin^2\frac{\theta}{2}\left[\frac{\mu}{6}J_3(\mu) - J_2(\mu) + \frac{1}{2\mu}J_1(\mu)\right]\right\}. \tag{B.11}$$

When $\theta = 0$, we obtain that $P_l^m(1) = (-)^m\left(l+\frac{1}{2}\right)^m J_m(0) = 0$ for $m \neq 0$, and $P_l^m(1) = 1$ for $m = 0$.

Eqs. (B.10) show the approximate relation between associated Legendre functions and Bessel functions of the first kind (of the integer order l, m of course). It is valid when the angle θ is not so large, the indices l's satisfy

$$0 \sim \frac{\theta}{4} \ll 2l+1 \ll \frac{48}{\theta^3}, \tag{B.12}$$

so that both $\frac{\mu}{6}\sin^2\frac{\theta}{2} \ll 1$ and $\frac{1}{2\mu}\sin^2\frac{\theta}{2} \ll 1$. MacDonald approximation is successfully generalized to small l's such as 0, 1, 2, $\cdots$.

As MacDonald discovered the approximation with traditional "series expansion and truncation" methods, later scientists all claimed that the approximation is only applicable for large l or $l+\frac{1}{2}$. We noticed that the key term, the polynomial

$$\frac{\Gamma(l+r+1)}{\Gamma(l-r+1)} \tag{B.13}$$

can be strictly reduced to

$$\left(l+\frac{1}{2}\right)^{2r} + A\left(l+\frac{1}{2}\right)^{2r-2} + B\left(l+\frac{1}{2}\right)^{2r-4} + \cdots + C \tag{B.14}$$

for $l = 0, 1$. As for $l \geq 2$, we have $\left(l+\frac{1}{2}\right)^2 \geq \frac{25}{4} \sim 7$ and $\left(l+\frac{1}{2}\right)^4 \geq \frac{625}{16} \sim 40$, which implies that the MacDonald approximation is not so bad even for small $l = 2, 3, 4, \cdots$. Later numerical results will confirm our prediction.

B.3 Numerical Simulation

To verify the validity of the generalized MacDonald approximation, we compare the 1st order, 2nd order approximation, with the exact value (numerical evaluation). [47]

Figs. B.1 – B.7 show $P_l^{-m}(\cos\theta)$, 1st order, 2nd order of the generalized MacDonald approximation as functions of the angle θ, for $l = 25,\ 50,\ 100$, $m = 0,\ 1,\ 2,\ \cdots,\ 7$ respectively, and corresponding error are also listed in the right-hand column.

As for $m = 0$, we find from Fig. B.1, that the error of generalized MacDonald's 1st order approximation is less than %5 for $\theta < 0.35 \sim 20°$, $\theta < 0.25 \sim 14°$, $\theta < 0.2 \sim 11°$, when $l = 25,\ 50,\ 100$ respectively. On the same figure, we also notice that the error of MacDonald's 2nd order approximation is less than %1 for $\theta < 0.35 \sim 20°$, which shows that the 2nd order approximation is perfect enough to evaluate arbitrary Legendre function in terms of Bessel functions. Similar results are obtained for $m = 1,\ 2,\ \cdots,\ 6$ in Figs. B.2 – B.7, and the angles, which corresponds to the error (1st order approximation) of %5, are all larger than $0.2 \sim 11°$.

We notice that the error grows with the increasing of the angel θ, for fixed l and m. It agrees well with Eqs. (B.10) that the leading error is proportional to $\sin^2\frac{\theta}{2}$ approximately.

Figs. B.8 – B.14 show $P_l^{-m}(\cos\theta)$, the 1st order, 2nd order generalized MacDonald approximation as functions of the indices l, for the angle $\theta = 5°$, $10°$, $20°$, the index $m = 0,\ 1,\ 2,\ \cdots,\ 7$ respectively, and the corresponding error are also listed.

As for $m = 0$, we find from Fig. B.8, that the error of MacDonald's 1st

order approximation is less than %5 for $l < 600$, $l < 200$, $l < 30$, when $\theta = 5°$, $10°$, $20°$ respectively. On the same figure, we also find that the error of MacDonald's 2nd order approximation is less than %1 for the same range of l, which shows that the 2nd order approximation is perfect enough to evaluate arbitrary Legendre function in terms of Bessel functions. Similar results are obtained for $m = 1, 2, \cdots, 6$ in Figs. B.9 - B.14, and the indices l, which corresponds to the error (1st order approximation) of %5, are all larger than those for $m = 0$.

We also notice that the error increases with the increasing of l, for fixed m and θ. It agrees well with Eqs. (B.10) that the leading error is related to $\frac{\mu}{6}$. Note that the affect of $\frac{1}{2\mu}$ term decreases with the increasing of l so that $\frac{\mu}{6}$ dominate.

Figs. B.15 - B.17 show $P_l^{-m}(\cos\theta)$, the 1st order, 2nd order generalized MacDonald approximation as functions of the indices m, for the angle $\theta = 5°$, $10°$, $20°$, the index $l = 25$, 50, and 100 respectively, and the corresponding error are also listed. Note that the error is shown in semi-log scale.

As for $\theta = 5°$, we find from Fig. B.15, that the absolute error of generalized MacDonald's 1st order approximation decreases with the increasing of m, while the relative error does not change too much. As for that of 2nd order approximation, similar trend is found in the same figure, and the accuracy is further improved. Similar results are obtained for $\theta = 10°$ and $20°$ in Fig. B.16 and B.17.

B.4 Conclusion

From our numerical results, MacDonald approximation is good, even for small l, contrary to the prevailing interpretation in the community.

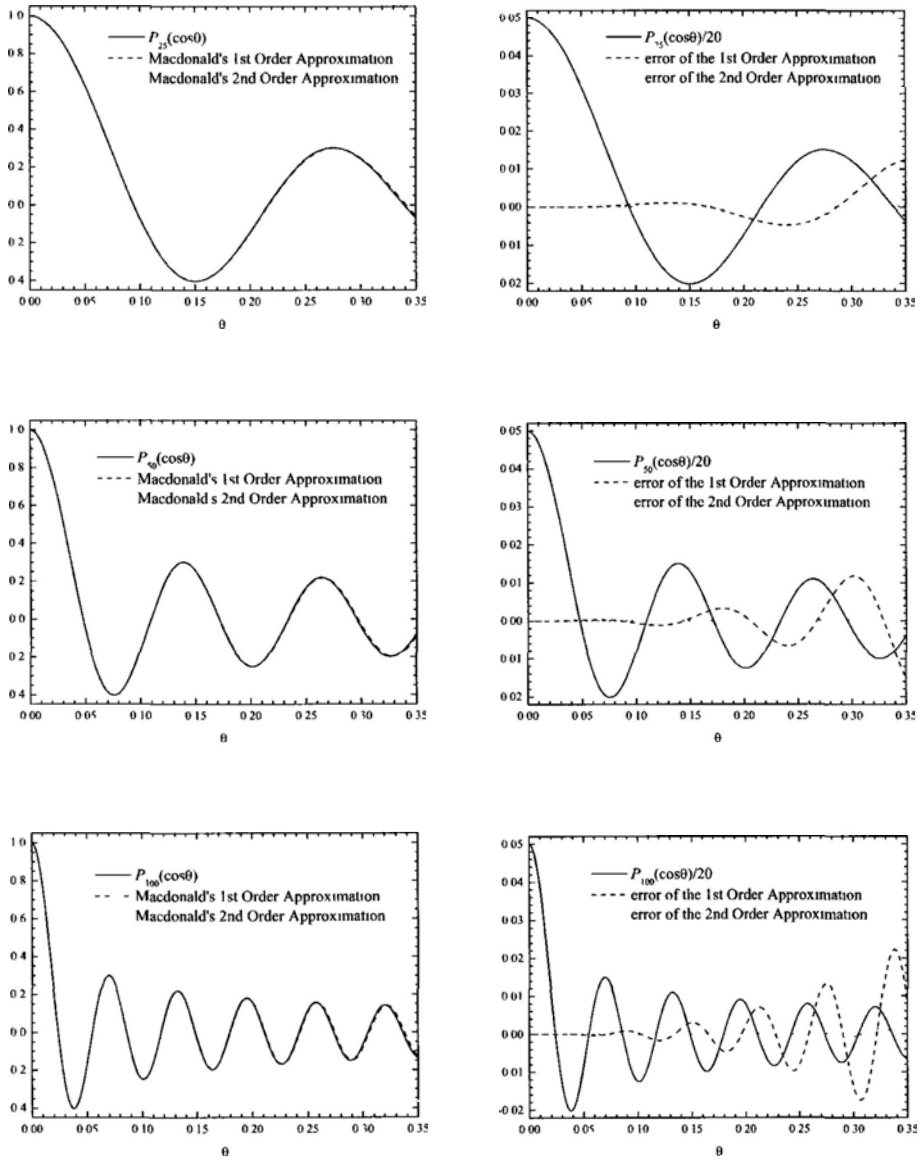

Figure B.1: Numerical evaluation of the functions $P_{25}(\cos\theta)$, $P_{50}(\cos\theta)$ and $P_{100}(\cos\theta)$, as well as the comparison with Macdonald's approximation.

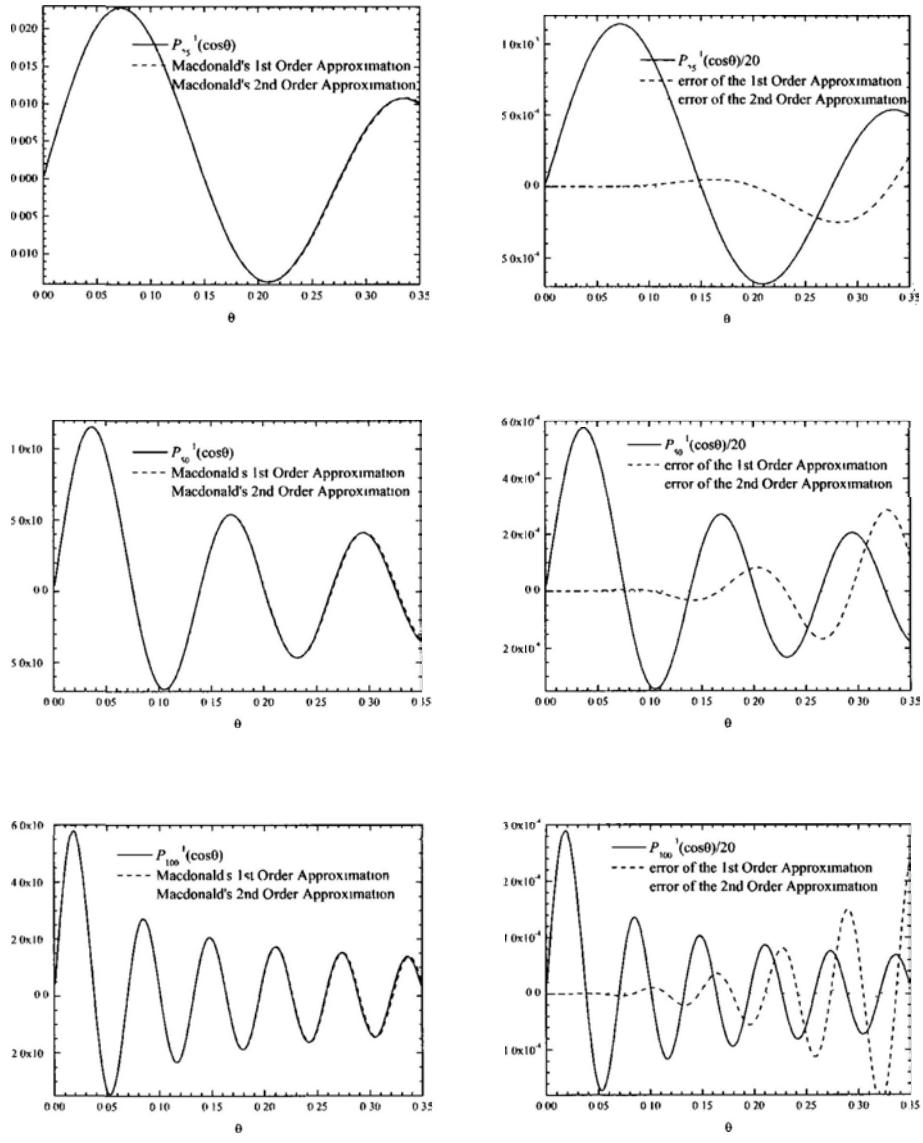

Figure B.2: Numerical evaluation of the functions $P_{25}^{-1}(\cos\theta)$, $P_{50}^{-1}(\cos\theta)$ and $P_{100}^{-1}(\cos\theta)$, as well as the comparison with Macdonald's approximation.

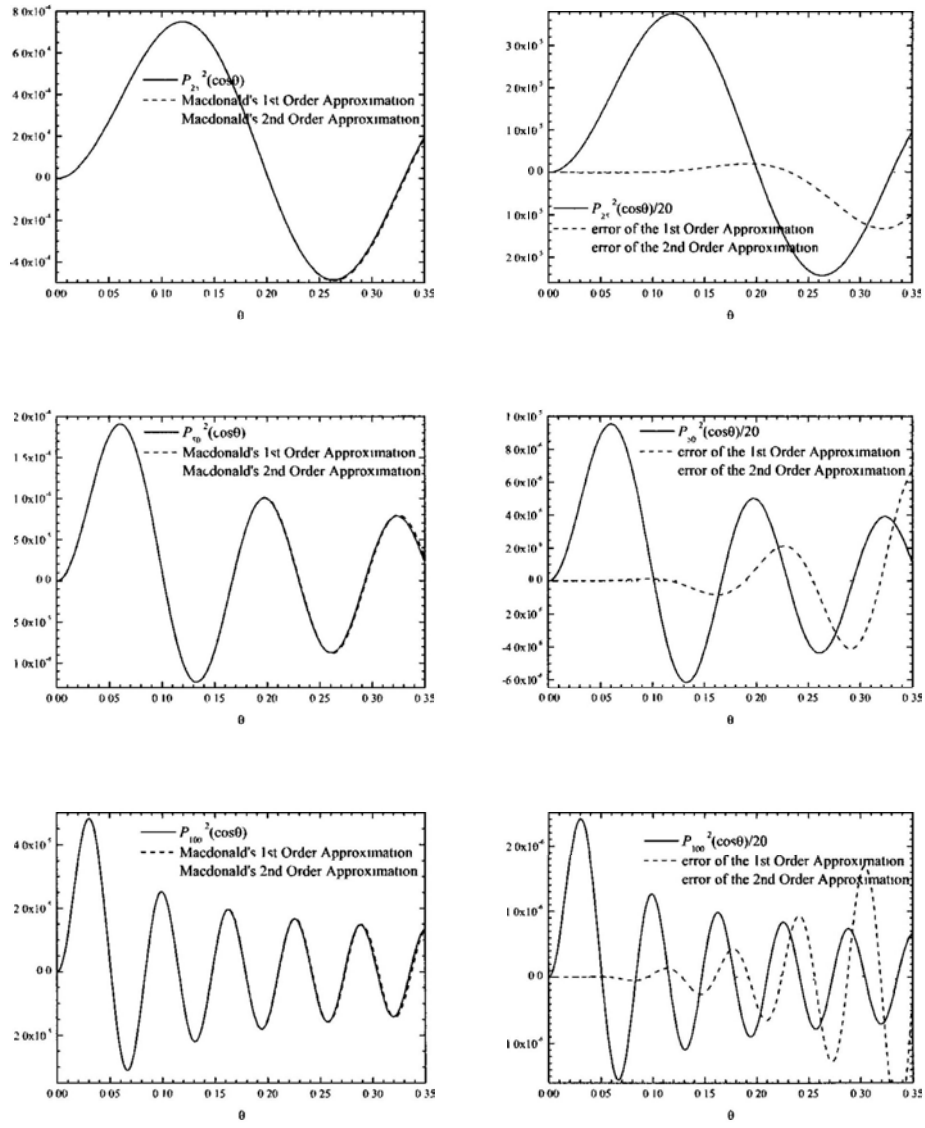

Figure B.3: Numerical evaluation of the functions $P_{25}^{-2}(\cos\theta)$, $P_{50}^{-2}(\cos\theta)$ and $P_{100}^{-2}(\cos\theta)$, as well as the comparison with Macdonald's approximation.

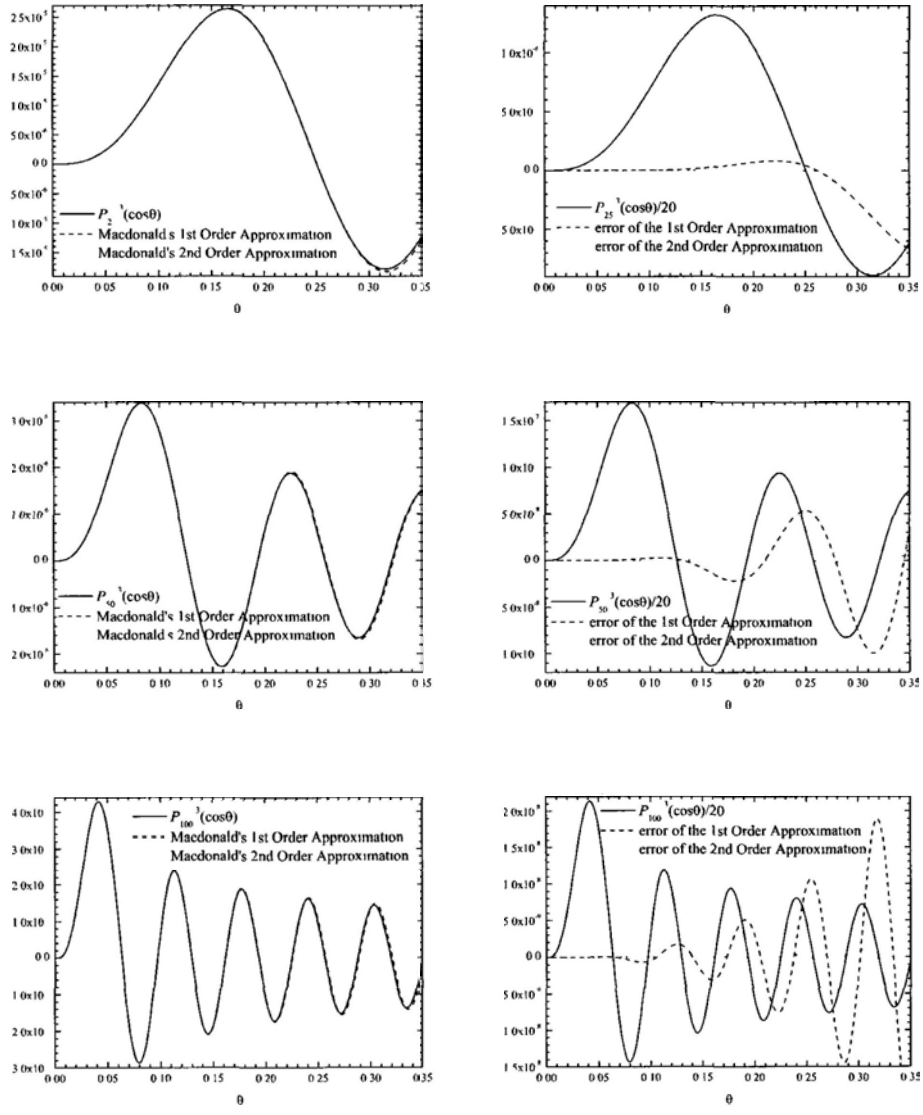

Figure B.4: Numerical evaluation of the functions $P_{25}^{-3}(\cos\theta)$, $P_{50}^{-3}(\cos\theta)$ and $P_{100}^{-3}(\cos\theta)$, as well as the comparison with Macdonald's approximation.

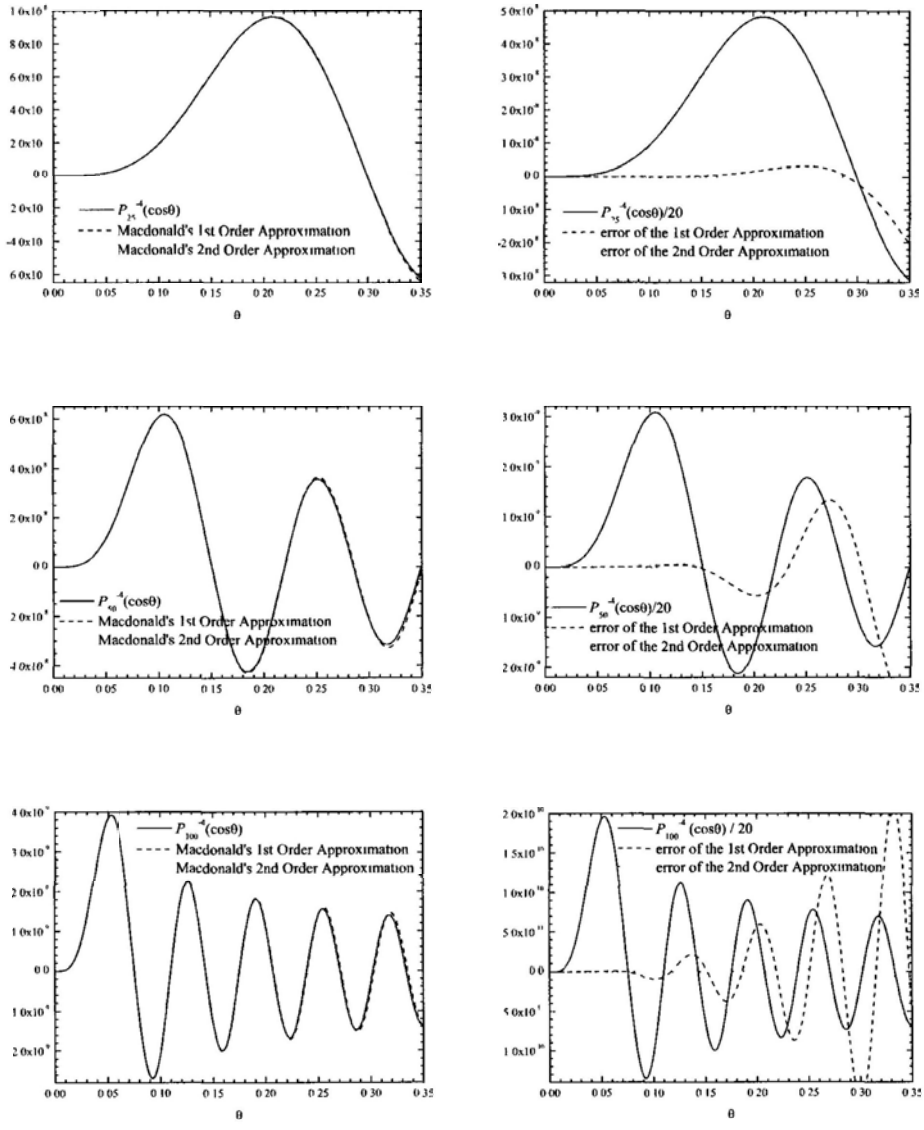

Figure B.5: Numerical evaluation of the functions $P_{25}^{-4}(\cos\theta)$, $P_{50}^{-4}(\cos\theta)$ and $P_{100}^{-4}(\cos\theta)$, as well as the comparison with Macdonald's approximation.

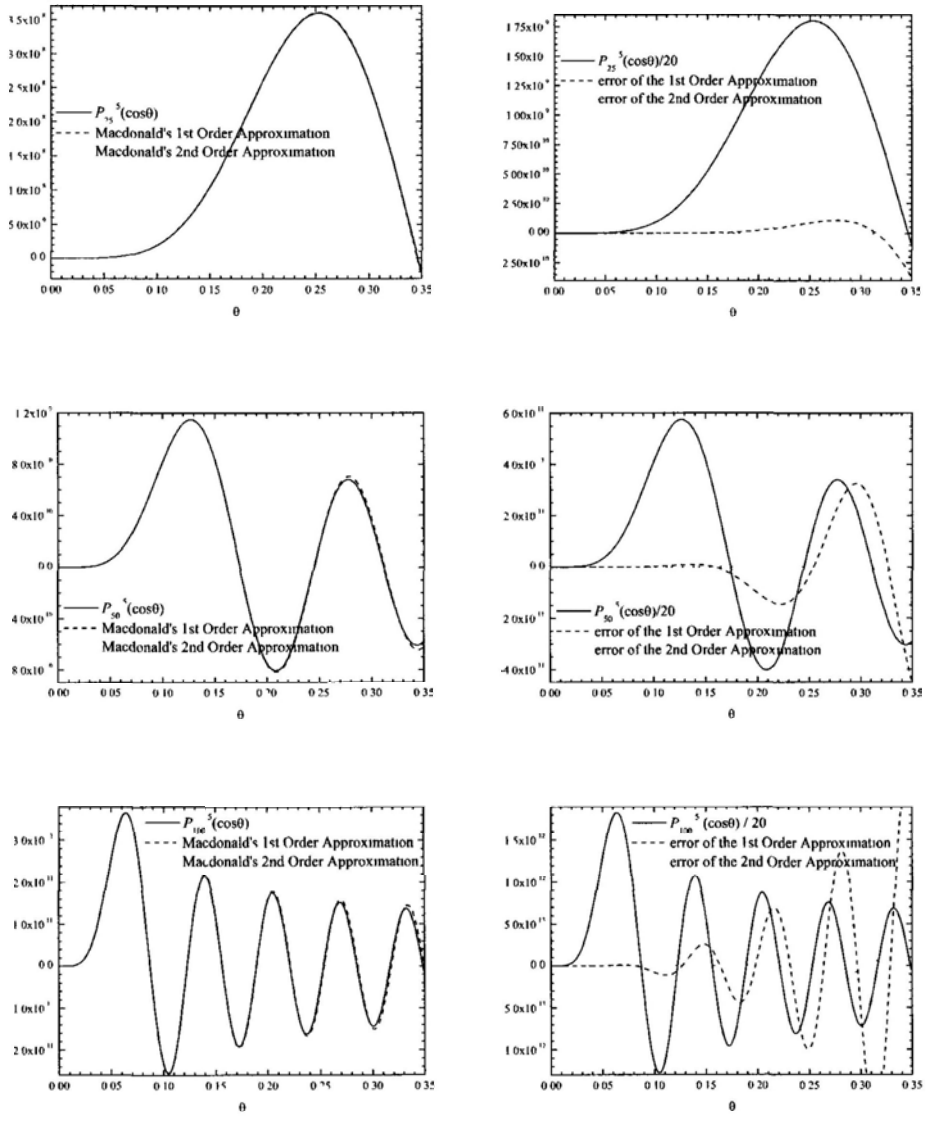

Figure B.6: Numerical evaluation of the functions $P_{25}^{-5}(\cos\theta)$, $P_{50}^{-5}(\cos\theta)$ and $P_{100}^{-5}(\cos\theta)$, as well as the comparison with Macdonald's approximation.

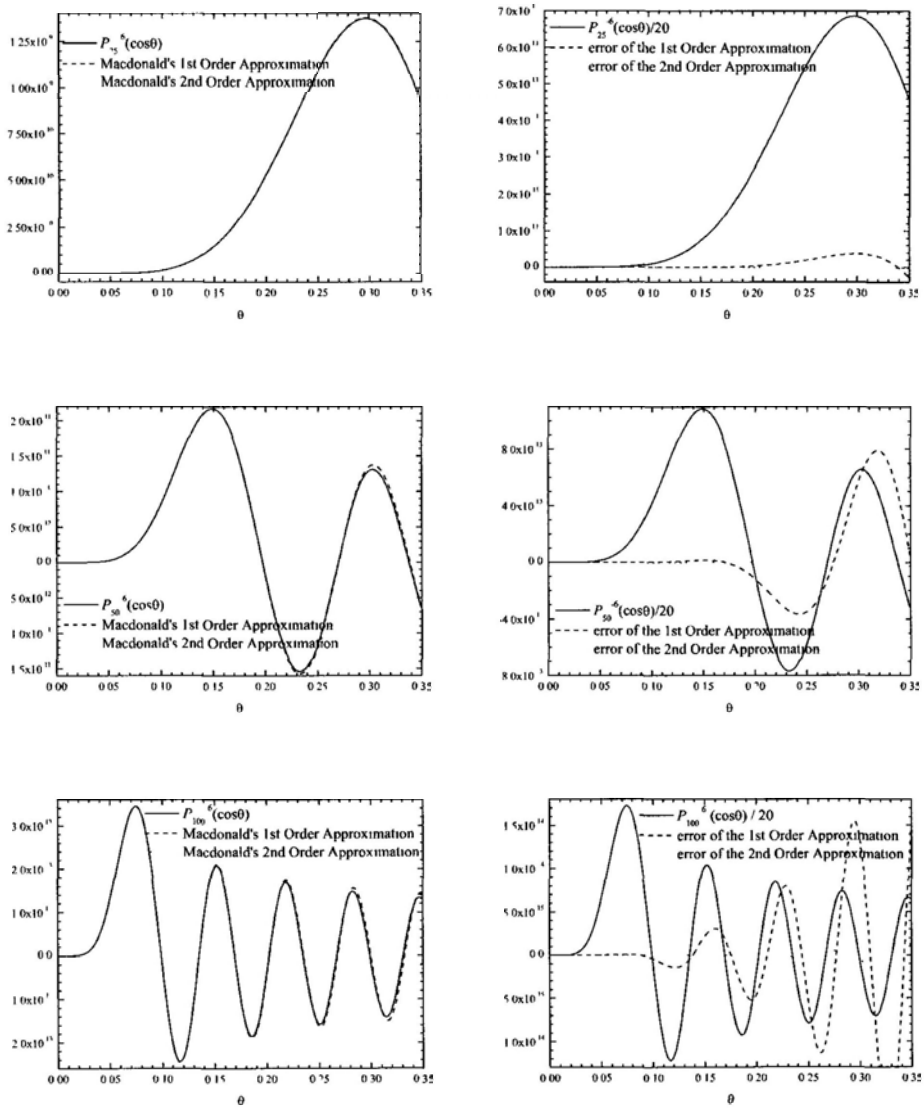

Figure B.7: Numerical evaluation of the functions $P_{25}^{-6}(\cos\theta)$, $P_{50}^{-6}(\cos\theta)$ and $P_{100}^{-6}(\cos\theta)$, as well as the comparison with Macdonald's approximation.

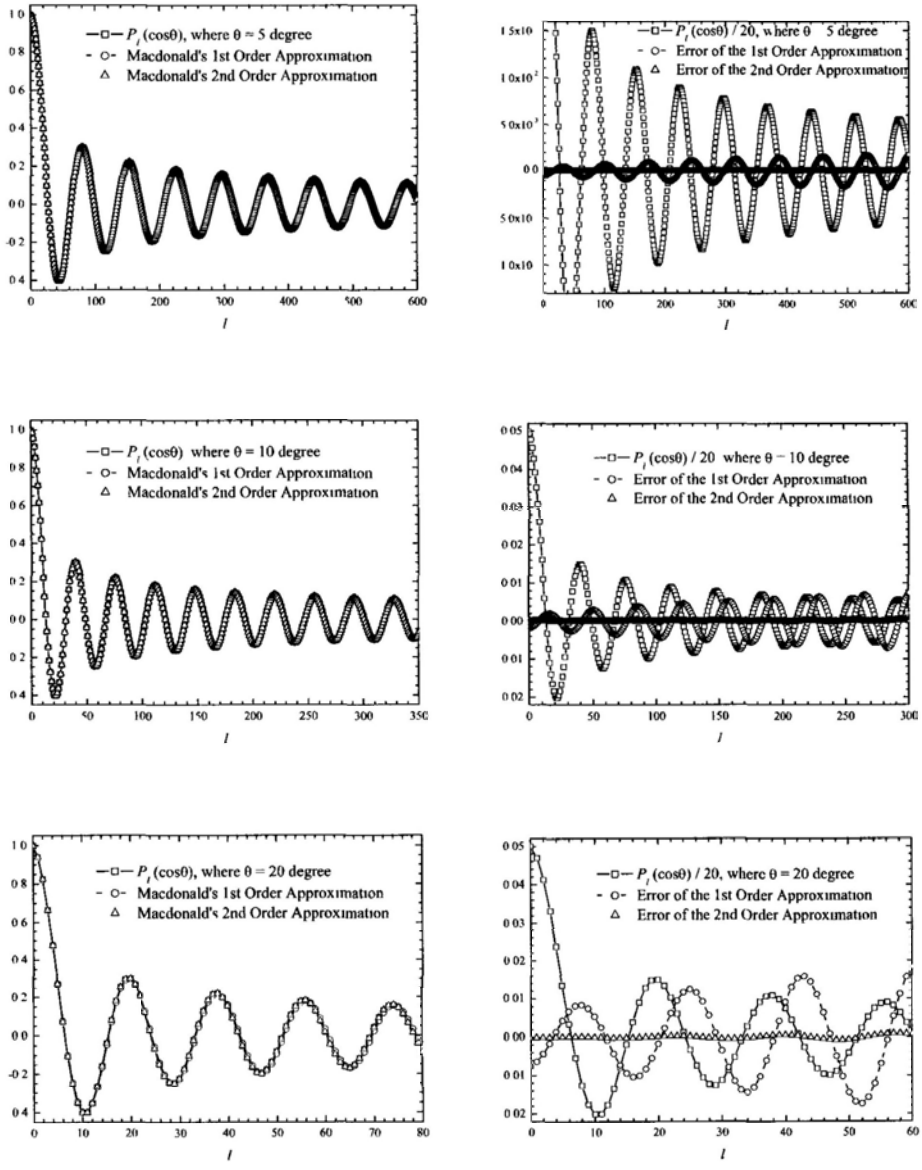

Figure B.8: Numerical evaluation of the functions $P_l(\cos 5°)$, $P_l(\cos 10°)$ and $P_l(\cos 20°)$, as well as the comparison with Macdonald's approximation.

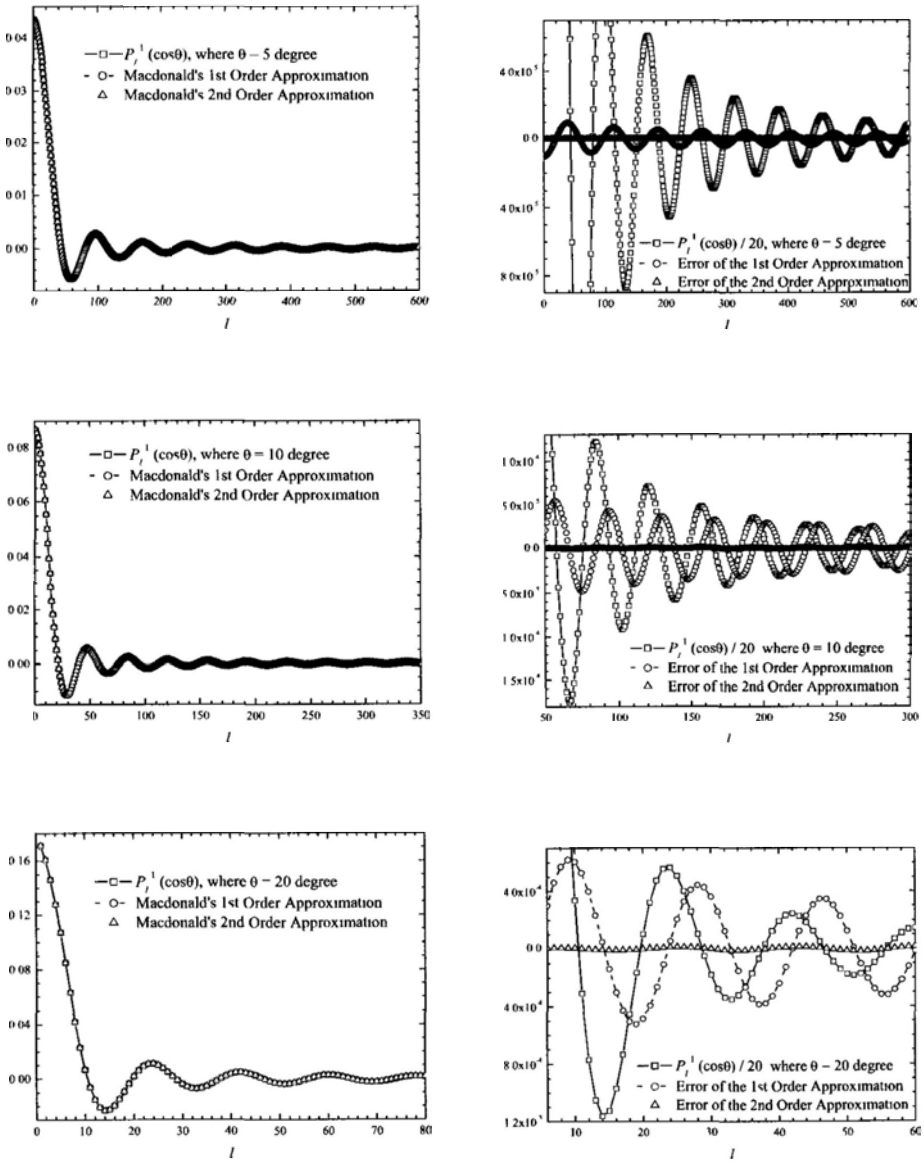

Figure B.9: Numerical evaluation of the functions $P_l^{-1}(\cos 5°)$, $P_l^{-1}(\cos 10°)$ and $P_l^{-1}(\cos 20°)$, as well as the comparison with Macdonald's approximation.

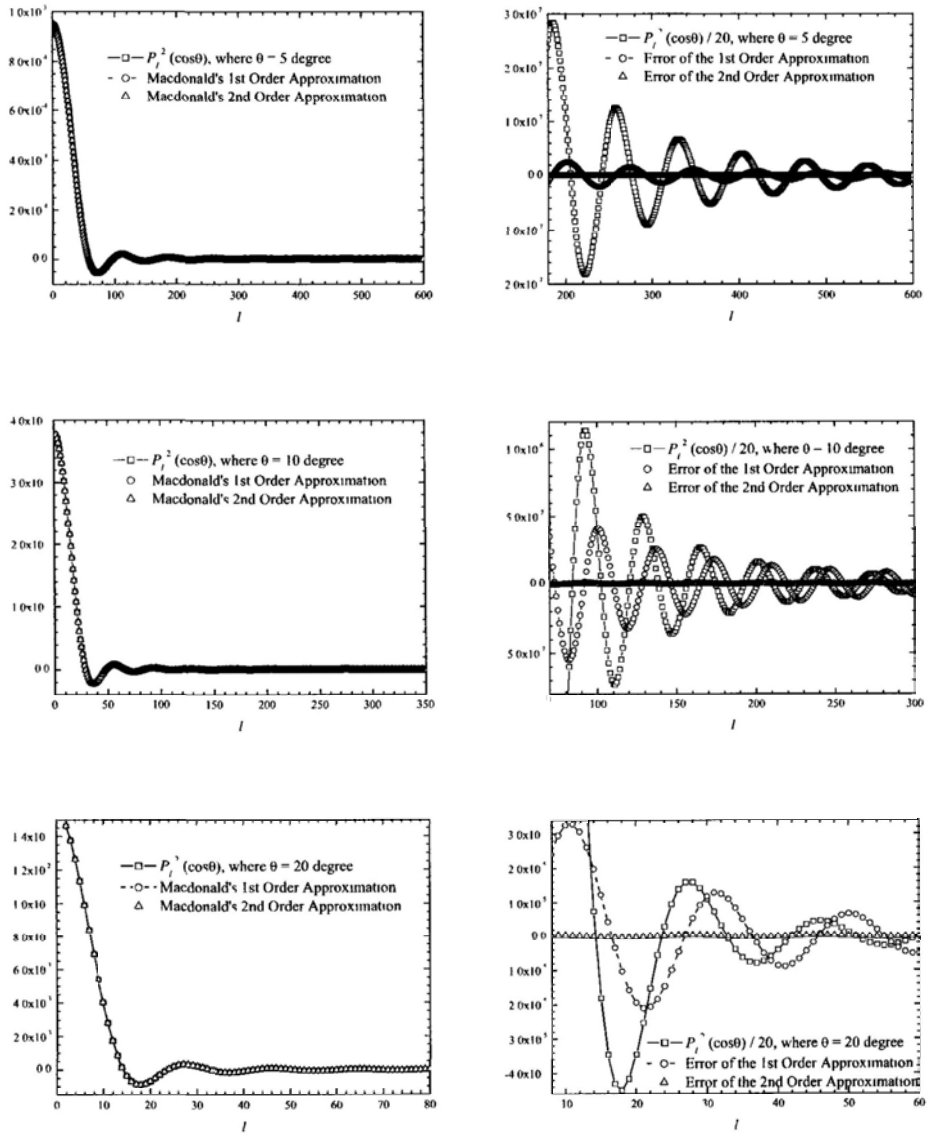

Figure B.10: Numerical evaluation of the functions $P_l^{-2}(\cos 5°)$, $P_l^{-2}(\cos 10°)$ and $P_l^{-2}(\cos 20°)$, as well as the comparison with Macdonald's approximation.

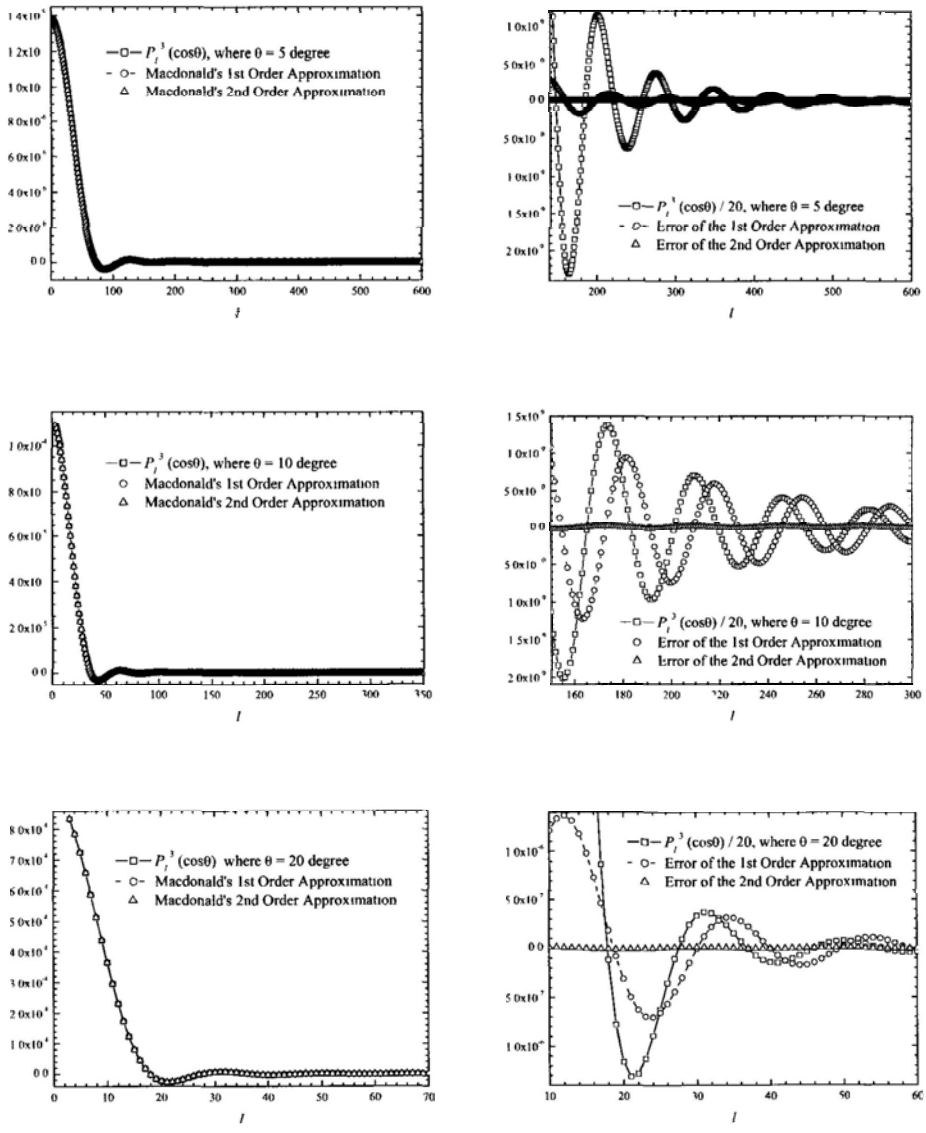

Figure B.11: Numerical evaluation of the functions $P_l^{-3}(\cos 5°)$, $P_l^{-3}(\cos 10°)$ and $P_l^{-3}(\cos 20°)$, as well as the comparison with Macdonald's approximation.

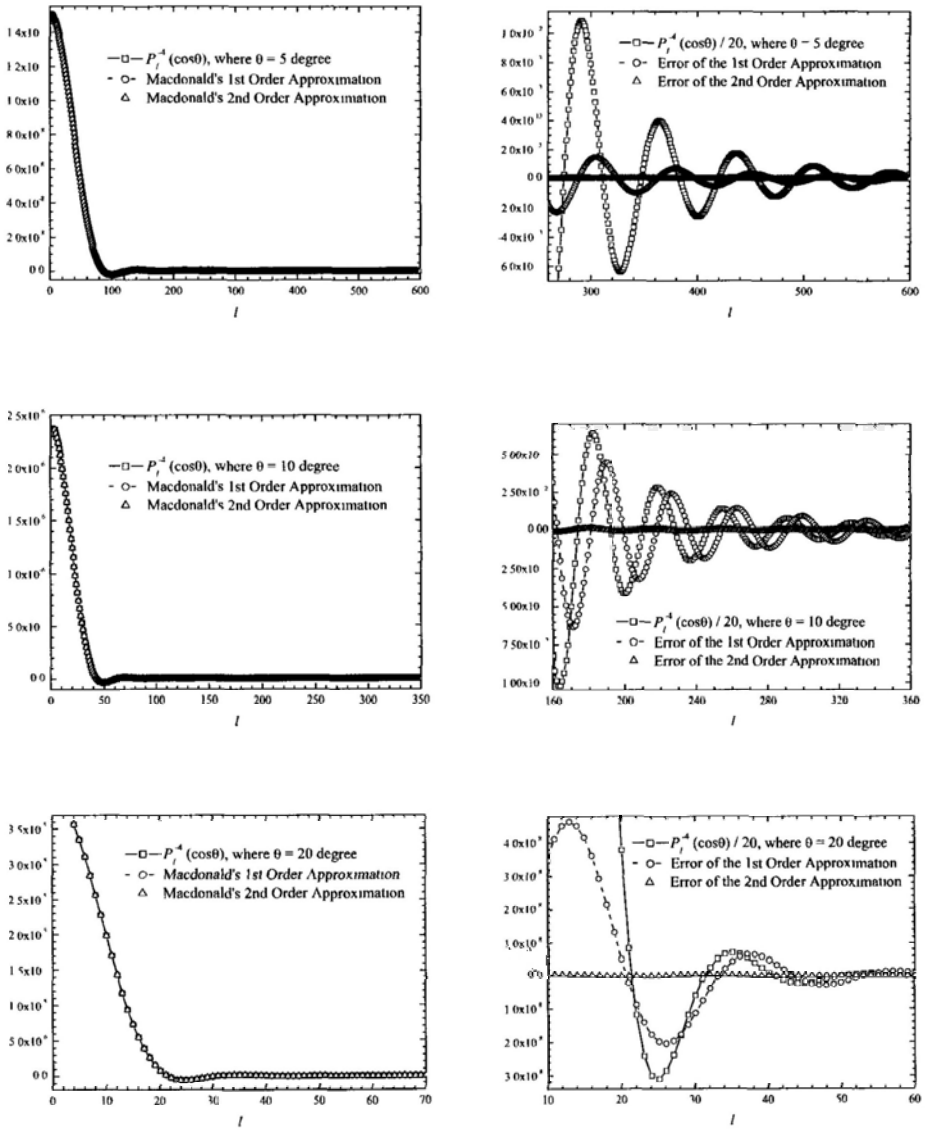

Figure B.12: Numerical evaluation of the functions $P_l^{-4}(\cos 5°)$, $P_l^{-4}(\cos 10°)$ and $P_l^{-4}(\cos 20°)$, as well as the comparison with Macdonald's approximation.

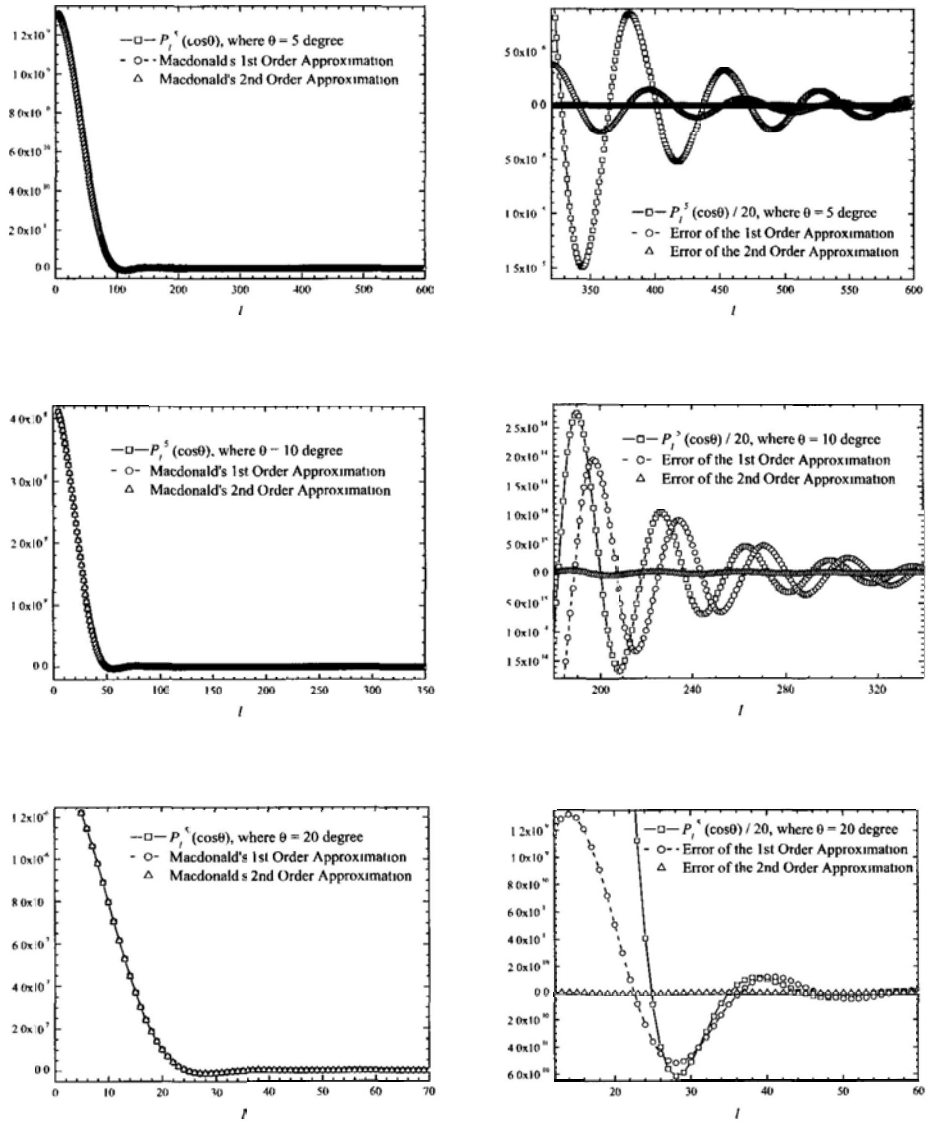

Figure B.13: Numerical evaluation of the functions $P_l^{-5}(\cos 5°)$, $P_l^{-5}(\cos 10°)$ and $P_l^{-5}(\cos 20°)$, as well as the comparison with Macdonald's approximation.

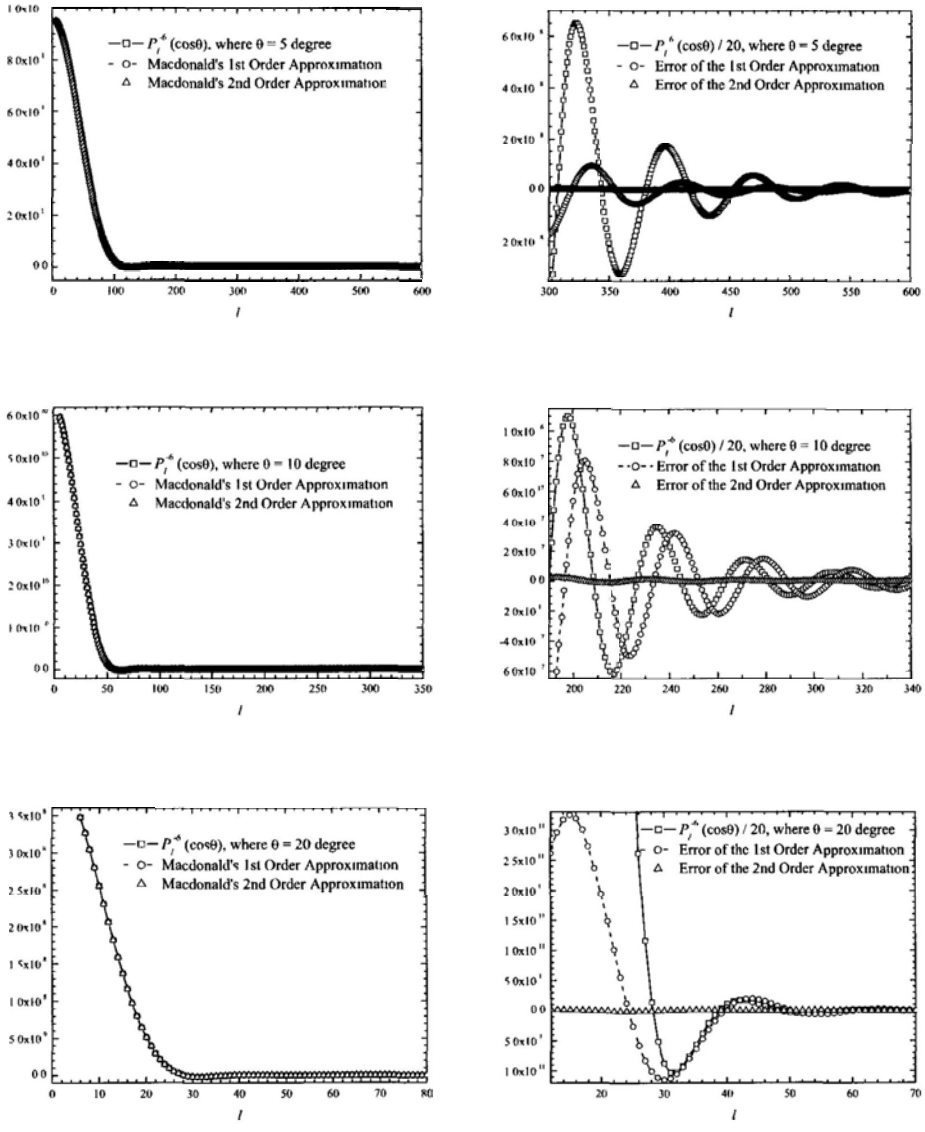

Figure B.14: Numerical evaluation of the functions $P_l^{-6}(\cos 5°)$, $P_l^{-6}(\cos 10°)$ and $P_l^{-6}(\cos 20°)$, as well as the comparison with Macdonald's approximation.

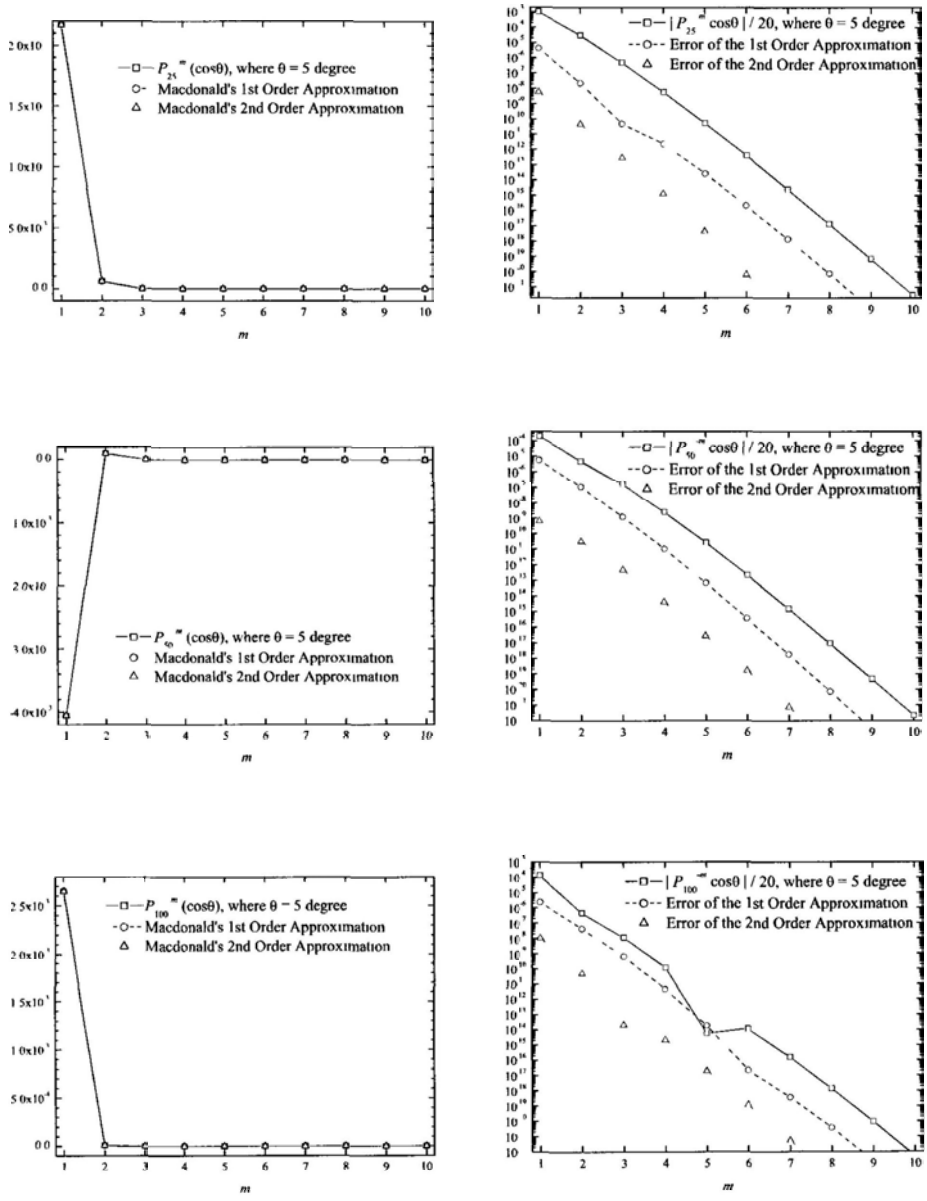

Figure B.15: Numerical evaluation of the functions $P_{25}^{-m}(\cos 5°)$, $P_{50}^{-m}(\cos 5°)$ and $P_{100}^{-m}(\cos 5°)$, as well as the comparison with Macdonald's approximation.

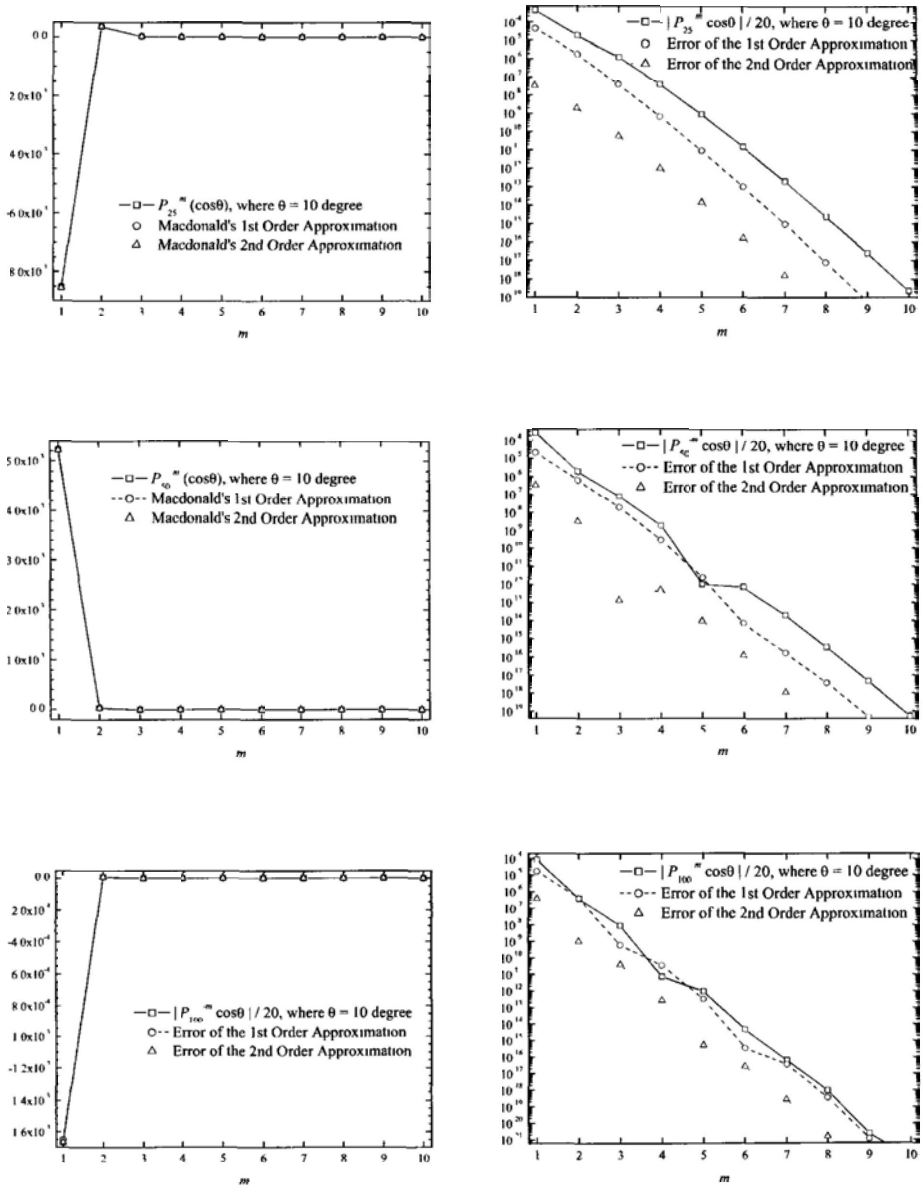

Figure B.16: Numerical evaluation of the functions $P_{25}^{-m}(\cos 10°)$, $P_{50}^{-m}(\cos 10°)$ and $P_{100}^{-m}(\cos 10°)$, as well as the comparison with Macdonald's approximation.

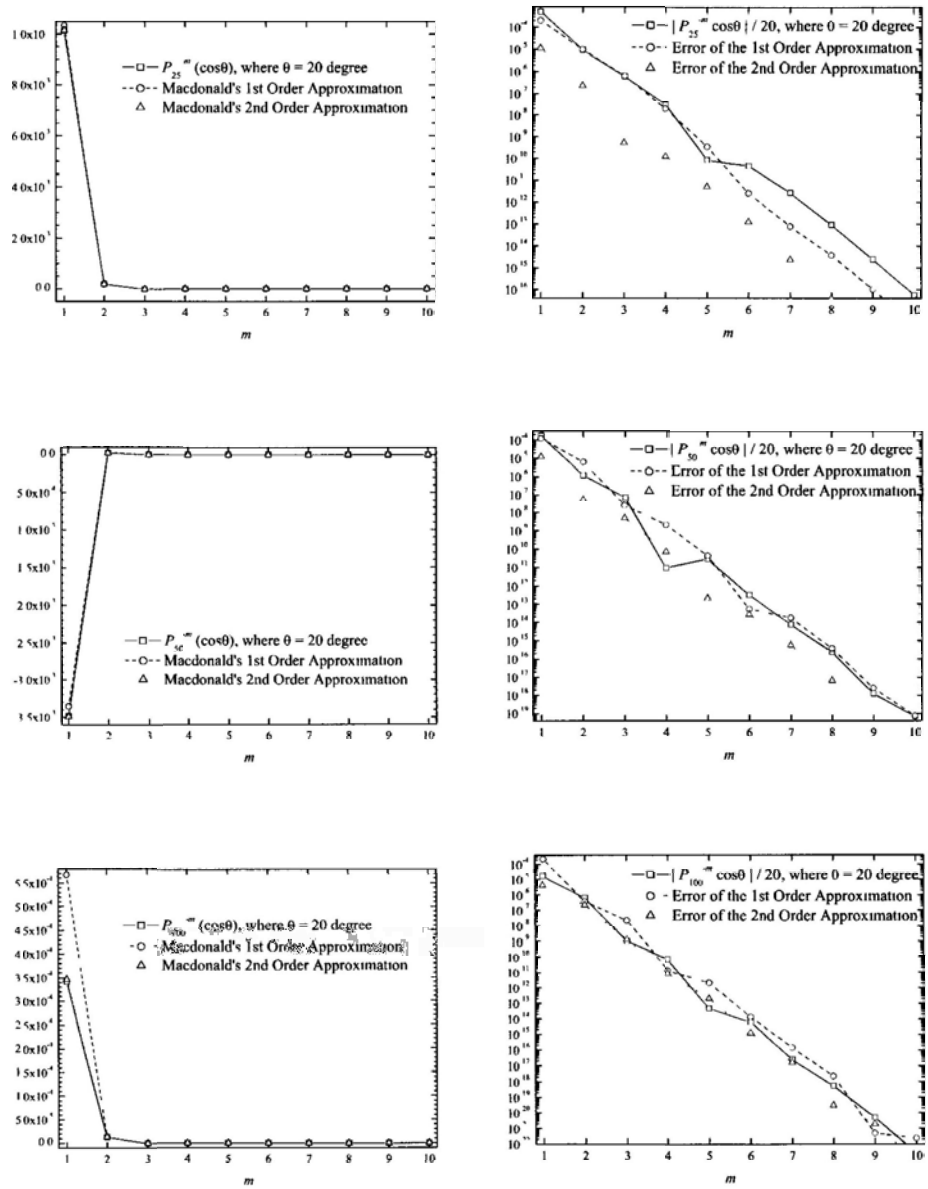

Figure B.17: Numerical evaluation of the functions $P_{25}^{-m}(\cos 20°)$, $P_{50}^{-m}(\cos 20°)$ and $P_{100}^{-m}(\cos 20°)$, as well as the comparison with Macdonald's approximation.

Appendix C

Recurrence Relations for Legendre Functions and Spherical Harmonics

The recurrence relations for Legendre functions and those for spherical harmonics are shown in this section. With these relations, we can manipulate the higher order terms of the approximate BSC's.

C.1 Recurrence Relations for Legendre Functions

From the generating function for Legendre functions, we have the following recurrence relations for Legendre Functions:

$$(2l+1)xP_l^m(x) = (l+m)P_{l-1}^m(x) + (l-m+1)P_{l+1}^m(x), \qquad \text{(C.1)}$$

$$(2l+1)\left(1-x^2\right)^{\frac{1}{2}} P_l^m(x) = P_{l-1}^{m+1}(x) - P_{l+1}^{m+1}(x), \tag{C.2}$$

$$\begin{aligned}(2l+1)\left(1-x^2\right)^{\frac{1}{2}} P_l^m(x) = (l-m+2)(l-m+1)P_{l+1}^{m-1}(x) \\ - (l+m)(l+m-1)P_{l-1}^{m-1}(x),\end{aligned} \tag{C.3}$$

and

$$(2l+1)(1-x^2)\frac{d}{dx}P_l^m(x) = (l+1)(l+m)P_{l-1}^m(x) - l(l-m+1)P_{l+1}^m(x). \tag{C.4}$$

C.2 Recurrence Relations for Spherical Harmonics

Based on the recurrence relations for Legendre Functions in the last section, and the definition of spherical harmonics by Jackson [24, Eq. (3.53)]

$$Y_{l,m}(\theta,\phi) = \sqrt{\frac{2l+1}{4\pi}\frac{(l-m)!}{(l+m)!}}P_l^m(\cos\theta)e^{im\phi}, \tag{C.5}$$

we have the following recurrence relations for spherical harmonics

$$\begin{aligned}\sqrt{2l+1}\cos\theta Y_{l,m}(\theta,\phi) = \sqrt{\frac{(l-m)(l+m)}{2l-1}}Y_{l-1,m}(\theta,\phi) \\ + \sqrt{\frac{(l-m+1)(l+m+1)}{2l+3}}Y_{l+1,m}(\theta,\phi),\end{aligned} \tag{C.6}$$

$$\sqrt{2l+1}\sin\theta e^{\imath\phi}Y_{l,m}(\theta,\phi) = \sqrt{\frac{(l-m-1)(l-m)}{2l-1}}Y_{l-1,m+1}(\theta,\phi) - \sqrt{\frac{(l+m+1)(l+m+2)}{2l+3}}Y_{l+1,m+1}(\theta,\phi), \quad \text{(C.7)}$$

$$\sqrt{2l+1}\sin\theta e^{-\imath\phi}Y_{l,m}(\theta,\phi) = \sqrt{\frac{(l-m+1)(l-m+2)}{2l+3}}Y_{l+1,m-1}(\theta,\phi) - \sqrt{\frac{(l+m-1)(l+m)}{2l-1}}Y_{l-1,m-1}(\theta,\phi), \quad \text{(C.8)}$$

and

$$\sqrt{2l+1}\sin\theta\frac{\partial}{\partial\theta}Y_{l,m}(\theta,\phi) = l\sqrt{\frac{(l-m+1)(l+m+1)}{2l+3}}Y^{m}_{l+1}(\theta,\phi) - (l+1)\sqrt{\frac{(l-m)(l+m)}{2l-1}}Y_{l-1,m}(\theta,\phi). \quad \text{(C.9)}$$

Bibliography

[1] J. W. S. Rayleigh. On the scattering of light by small particles. *Philos. Mag.*, 41:447 454, 1871.

[2] G Mie. Beiträge zur Optik Trüber Medien, Speziell Kolloidaler Metallösungen. *Ann. Phys.*, 25:377–452, 1908.

[3] H. C. van de Hulst. *Light scattering by small particles.* Structure of matter series. Wiley, New York, 1957.

[4] M. Kerker. *The scattering of light, and other electromagnetic radiation*, volume 16 of *Physical chemistry, a series of monographs.* Academic Press, New York, 1969.

[5] G. Gouesbet and G. Gréhan. Generalized Lorenz-Mie theories, from past to future. *Atom. Sprays*, 10(3–5):277–333, May–October 2000.

[6] M. Kerker. Lorenz–Mie scattering by spheres: Some newly recognized phenomena. *Aerosol Science and Technology*, 1(3):275–291, 1982.

[7] C. F. Bohren and D. R. Huffman. *Absorption and scattering of light by small particles.* Wiley, New York, 1983.

[8] P. W. Barber and R. K. Chang. *Optical effects associated with small particles*, volume 1 of *Advanced series in applied physics*. World Scientific, Singapore, 1988.

[9] N. A. Logan. Survey of some early studies of the scattering of plane waves by a sphere. In M. Kerker, editor, *Selected Papers on Light Scattering*, volume 951 of *Proceedings of SPIE*, pages 3–15. SPIE, International Society for Optical Engineering, Bellingham, Wash., 1988.

[10] G. Gouesbet. Generalized Lorenz-Mie theory and applications. *Part. Part. Syst. Charact.*, 11(1):22–34, February 1994.

[11] M. I. Mishchenko and L. D. Travis. Gustav Mie and the evolving subject of light scattering by particles. In Teruyuki Nakajima and Marcia Akemi Yamasoe, editors, *Current Problems in Atmospheric Radiation (IRS 2008): Proceedings of the International Radiation Symposium (IRC/IAMAS)*, volume 1100 of *AIP Conference Proceedings*, pages 11–15. American Institute of Physics, 2009.

[12] H. M. Tzeng, K. F. Wall, M. B. Long, and R. K. Chang. Laser emission from individual droplets at wavelengths corresponding to morphology-dependent resonances. *Opt. Lett.*, 9(11):499–501, November 1984.

[13] S. M. Spillane, T. J. Kippenberg, and K. J. Vahala. Ultra-threshold Raman laser using a spherical dielectric microcavity. *Nature*, 415(6872):621–623, February 2002.

[14] A. R. Jones. Light scattering for particle characterization. *Progress in Energy and Combustion Science*, 25(1):1–53, 1999.

[15] X.-C. Wu, G. Gréhan, Siegfried Meunier-Guttin-Cluzel, L.-H. Chen, and K.-F. Cen. Sizing of particles smaller than 5 μm in digital holographic microscopy. *Opt. Lett.*, 34(6):857–859, March 2009.

[16] A. J. Campillo, J. D. Eversole, and H.-B. Lin. Cavity quantum electrodynamic enhancement of stimulated emission in microdroplets. *Phys. Rev. Lett.*, 67(4):437–440, July 1991.

[17] J. A. Lock. Improved Gaussian beam-scattering algorithm. *Appl. Opt.*, 34(3), January 1995.

[18] C. Mund and R. Zellner. Optical levitation of single microdroplets at temperatures down to 180 K. *ChemPhysChem*, 4(6):630–638, June 2003.

[19] A. Ashkin and J. M. Dziedzic. Observation of resonances in the radiation pressure on dielectric spheres. *Phys. Rev. Lett.*, 38(23):1351–1354, June 1977.

[20] J.-Z. Zhang, D. H. Leach, and R. K. Chang. Photon lifetime within a droplet: temporal determination of elastic and stimulated Raman scattering. *Opt. Lett.*, 13(4):270–272, April 1988.

[21] G. Gouesbet, B. Maheu, and G. Gréhan. Light scattering from a sphere arbitrarily located in a Gaussian beam, using a Bromwich formulation. *J. Opt. Soc. Am. A*, 5(9):1427–1443, September 1988.

[22] E. E. M. Khaled, S. C. Hill, and P. W. Barber. Scattered and internal intensity of a sphere illuminated with a Gaussian beam. *IEEE Trans. Antennas Propag.*, 41(3):295–303, March 1993.

[23] S C. Hill and R. E. Benner. Morphology-dependent resonances. In P. W. Barber and R. K Chang, editors, *Optical effects associated with small particles*, page 40. World Scientific, Singapore, 1988.

[24] J. D. Jackson. *Classical electrodynamics.* John Wiley and Sons, Inc, New York, 3rd edition, 1999.

[25] R. K. Chang and A. J. Campillo, editors. *Optical processes in microcavities*, volume 3 of *Advanced series in applied physics*, pages 1–76. World Scientific. Singapore, 1996. Optical Processes in Microcavities — The Role of Quasinormal Modes.

[26] C. C. Lam, P. T. Leung, and K. Young. Explicit asymptotic formulas for the positions, widths, and strengths of resonances in Mie scattering. *J. Opt. Soc. Am. B*, 9(9):1585–1592, September 1992.

[27] M. Abramowitz and I. A. Stegun, editors. *Handbook of mathematical functions with formulas, graphs, and mathematical tables*, volume 55 of *United States. National Bureau of Standards. Applied mathematics series*, page 366. U.S. Govt. Print. Off., Washington, 1964.

[28] M. J. Lighthill, editor. *Introduction to Fourier Analysis and Generalized Fuctions*, page 22. Cambridge U. Press, 1964.

[29] H.-B. Lin, J. D. Eversole, A. J Campillo, and John P. Barton. Excitation localization principle for spherical microcavities. *Opt. Lett.*, 23(24):1921–1923, December 1998.

[30] John P. Barton. Effects of surface perturbations on the quality and the focused-beam excitation of microsphere resonance. *J. Opt. Soc. Am. A*, 16(8):1974–1980, August 1999.

[31] James A. Lock. Excitation of morphology-dependent resonances and van de Hulst's localization principle. *Opt. Lett.*, 24(7):427–429, April 1999.

[32] G. Gouesbet. Generalized Lorenz-Mie theories, the third decade: A perspective. *Journal of Quantitative Spectroscopy and Radiative Transfer*, 110(14–16):1223–1238, September–November 2009.

[33] James A. Lock and G. Gouesbet. Generalized Lorenz-Mie theory and applications. *Journal of Quantitative Spectroscopy and Radiative Transfer*, 110(11):800–807, July 2009.

[34] Gérard Gouesbet and James A. Lock. Rigorous justification of the localized approximation to the beam-shape coefficients in generalized Lorenz-Mie theory. II. off-axis beams. *J. Opt. Soc. Am. A*, 11(9):2516–2525, September 1994.

[35] G. Gouesbet. Validity of the localized approximation for arbitrary shaped beams in the generalized Lorenz-Mie theory for spheres. *J. Opt. Soc. Am. A*, 16(7):1641–1650, July 1999.

[36] H. M. Lai, W. Y. Wong, and W. H. Wong. Extinction paradox and actual power scattered in light beam scattering: a two-dimensional study. *J. Opt. Soc. Am. A*, 62:2324–2333, 2004.

[37] I. S. Gradshteyn and I. M.Ryzhik. *Table of Integrals, Series, and Products*, page 1005. Academic Press, New York and London, 4th edition, 1965. Eq.(**8.733** 4).

[38] I. S. Gradshteyn and I. M.Ryzhik. *Table of Integrals, Series, and Products*, page 1006. Academic Press, New York and London, 4th edition, 1965. Eq.(**8.735** 5).

[39] I. S. Gradshteyn and I. M.Ryzhik. *Table of Integrals, Series, and Products*, page 795. Academic Press, New York and London, 4th edition, 1965. Eq.(**7.121**).

[40] I. S. Gradshteyn and I. M.Ryzhik. *Table of Integrals, Series, and Products*, page 1003. Academic Press, New York and London, 4th edition, 1965. Eq.(**8.722** 1).

[41] G. N. Watson. *A treatise on the theory of Bessel functions.* Cambridge University Press, Cambridge [England], 2nd edition, 1944.

[42] H. M. Macdonald. Zeroes of the spherical harmonic $P_n^m(\mu)$ considered as a function of n. *Proc. London Math. Soc.*, xxxi:264–285, May 1899.

[43] H. M. Macdonald. Formulæ for the spherical harmonic $P_n^{-m}(\mu)$, when $1-\mu$ is a small quantity. *Proc. London Math. Soc.*, 13:220–221, February 1914. 2nd Series.

[44] E. T. Whittaker. Hector Munro MacDonald. 1865-1935. *Obituary Notices of Fellows of the Royal Society*, 1(4):550–558, December 1935.

[45] I. S. Gradshteĭn and I. M. Ryzhik. *Table of Integrals, Series, and Products.* Academic Press, San Diego, 7th edition, 2007.

[46] M. Abramowitz and I. A. Stegun, editors. *Handbook of mathematical functions with formulas, graphs, and mathematical tables*, volume 55 of *United States. National Bureau of Standards. Applied mathematics series*. U.S. Govt. Print. Off., Washington, 1964.

[47] A. M. Mintairov, Y. Chu, and Y. He, etc. High-spatial-resolution near-field photoluminescence and imaging of whispering-gallery modes in semiconductor microdisks with embedded quantum dots. *Phys. Rev. B*, 77(19):195322, May 2008.